



Volume 36, Number 2, June 2010.

Mobility & Vehicle Mechanics

*International Journal for Vehicle Mechanics, Engines
and Transportation Systems*

ISSN 1450 – 5304

Editors: Prof. dr Aleksandra Janković, Prof. dr Čedomir Duboka UDC 621+ 629(05)=802.0

Ile Mircheski Tatjana Kandikjan Petar Simonovski	VIRTUAL TESTING AND EXPERIMENTAL VERIFICATION OF SEAT COMFORT IN DRIVER'S SEAT FOR PASSENGER AUTOMOBILE	7-20
Popa Dinel Parlac Sebastian Dejanu Marcel	THEORETICAL AND EXPERIMENTAL STUDY OF THE MECHANISMS USED IN THE CONSTRUCTION OF PLANETARY TRANSMISSION OF HYBRID CARS	21-36
Lilo Kunchev Nikolay Pavlov	COMPARATIVE ANALYSIS ON MATHEMATICAL MODELS DESCRIBING VIBRATIONS OF AUTOMOTIVE INDEPENDENT SUSPENSIONS	37-52
Catalin-Adrian Neacsu Mariana Ivanescu Ion Tabacu	NUMERICAL SIMULATION OF AIR FLOW THROUGH TWO DIFFERENT SHAPED AIR VENTS	53-65



UNIVERSITY OF KRAGUJEVAC – FACULTY OF MECHANICAL ENGINEERING
SERBIAN SOCIETY OF AUTOMOTIVE ENGINEERS



M V M

Mobility Vehicle Mechanics

Editors: Prof. dr Aleksandra Janković; Prof. dr Čedomir Duboka

MVM Editorial Board
University of Kragujevac
Faculty of Mechanical Engineering
Sestre Janjić 6, 34000 Kragujevac, Serbia
Tel.: +381/34/335990; Tel.: 336002; Fax: + 381/34/333192

Prof. Dr **Belingardi Giovanni**
Politecnico di Torino
Torino, ITALY

Dr Ing. **Čučuz Stojan**
Visteon corporation,
Novi Jicin,
CZECH REPUBLIC

Prof. Dr **Demić Miroslav**
Faculty of Mech. Eng. Kragujevac
Department for Motor Vehicles
and Motors, Kragujevac,
SERBIA

Prof. Dr **Fiala Ernest**
WIEN, OESTERREICH

Prof. Dr **Gillespie D. Thomas**
University of Michigan,
Ann Arbor, Michigan, USA

Prof. Dr **Grujović Aleksandar**
Faculty of Mech. Eng. Kragujevac
SERBIA

Prof. Dr **Knapezyk Josef**
Politechniki Krakowskiej
Krakow, POLAND

Prof. Dr **Krstić Božidar**
Faculty of Mech. Eng. Kragujevac
Department for Motor Vehicles
and Motors, Kragujevac,
SERBIA

Prof. Dr **Mariotti G. Virzi**
Universita degli Studi di
Palermo, Dipartimento di
Meccanica ed Aeronautica
Palermo, ITALY

Prof. Dr **Pešić Radivoje**
Faculty of Mech. Eng. Kragujevac
Department for Motor Vehicles
and Motors, Kragujevac,
SERBIA

Prof. Dr **Petrović Stojan**
Faculty of Mech. Eng. Belgrade
SERBIA

Prof. Dr **Radonjić Dragoljub**
Faculty of Mech. Eng. Kragujevac
Department for Motor Vehicles
and Motors, Kragujevac,
SERBIA

Prof. Dr **Radonjić Rajko**
Faculty of Mech. Eng.
Kragujevac
Department for Motor Vehicles
and Motors, Kragujevac,
SERBIA

Prof. Dr **Spentzas Constantinos**
N. National Technical
University
GREECE

Prof. Dr **Todorović Jovan**
Faculty of Mech. Eng. Belgrade
SERBIA

Prof. Dr **Toliskyj Vladimir E.**
Academician NAMI, Moscow
RUSSIA

Prof. Dr **Teodorović Dušan**
Faculty of Traffic and Transport
Engineering, Belgrade
SERBIA

Prof. Dr **Veinović Stevan**
Faculty of Mech. Eng.
Kragujevac
SERBIA

For Publisher: Prof. dr Miroslav Babić, dean, Faculty of Mechanical Engineering, Kragujevac
Ordering: Vesna Maksimović
Printed by: PRESprint, Kamenička 4, Kragujevac
tel: + 381/ 34/ 335990 / 607

Publishing of this Journal is financially supported from:
Ministry of Science and Tehnological Development, Belgrade, Serbia
Center of Traffic Safety, Faculty of Mechanical Engineering, Kragujevac

NOTIFICATION TO AUTHORS

The Journal MVM publishes original papers which have not been previously published in other journals. This is responsibility of the author. The authors agree that the copyright for their article is transferred to the publisher when the article is accepted for publication.

The language of the Journal is English.

Journal *Mobility & Vehicles Mechanics* is at the SSCI list.

All submitted manuscripts will be reviewed. Entire correspondence will be performed with the first-named author.

Authors will be notified of acceptance of their manuscripts, if their manuscripts are adopted. Authors are requested to participate in paper publishing expenses as it is described below:

For Native Authors: 6 pages are provided free of charge, written according to editor's given instructions. Each extra page will be charged with RSD 800 per page.

For Foreign Authors: 6 pages are provided free of charge, written according to editor's given instructions. Each extra page will be charged with €20 per page.

INSTRUCTIONS TO AUTHORS:

Abstract is a separate Word document, "ABSTRACT". Native authors should write the abstract in both languages (Serbian and English). The abstracts of foreign authors will be translated in Serbian for free.

This document should include the following: 1) author's name, affiliation and title, the first-named author's address and e-mail – for correspondence, 2) working title of the paper, 3) abstract containing no more than 100 words, 4) key words.

The manuscript is the separate file, „TEXT“ which includes appendices and figures involved within the text. At the end of the paper, a reference list and eventual acknowledgements should be given. References to published literature should be quoted in the text brackets and grouped together at the end of the paper in numerical order.

Paper size:	Max 16 pages of B5 format, excluding abstract
Text processor:	Microsoft Word
Margins:	left/right: mirror margin, inside: 2.5 cm, outside: 2 cm top: 2.5 cm, bottom: 2 cm
Font:	Times New Roman, 10 pt
Paper title:	Uppercase, bold, 11 pt
Chapter title:	Uppercase, bold, 10 pt
Subchapter title:	Lowercase, bold, 10 pt
Table and chart width:	max 125 mm
Figure and table title:	Figure _: Times New Roman, italic 10 pt Table _: Times New Roman, italic 10 pt
Manuscript submission:	application should be sent to the following e-mail: <u>mvm@kg.ac.rs</u> ; <u>alex@kg.ac.rs</u> or posted to address of the Journal:

**University of Kragujevac – Faculty of Mechanical Engineering Kragujevac
International Journal M V M
Sestre Janjić 6, 34000 Kragujevac, Serbia**

Journal editorial board will send to the first-named author a free copy of the Journal offprint. Authors will have a discount of 50% of the price for current year.

OBAVEŠTENJE AUTORIMA

Časopis MVM objavljuje originalne radove koji nisu prethodno objavljeni u drugim časopisima, što je odgovornost autora. Za rad koji je prihvaćen za štampu, prava umnožavanja pripadaju izdavaču.

Jezik na kojem je časopis napisan je engleski.

Časopis *Mobility & Vehicles Mechanics* se nalazi na SSCI listi.

Svi prispeli radovi se recenziraju. Sva komunikacija se obavlja sa prvim autorom.

Po dobijanju pozitivne recenzije autor-autori participiraju u troškovima izdavanja rada i to:

Domaći autori mogu besplatno da objave do 6 strana ukupno, uređenih prema uputstvu redakcije. Za svaku daljnu stranu, autor plaća 800 dinara po strani.

Strani autori mogu besplatno da objave do 6 strana ukupno, uređenih prema uputstvu redakcije. Za svaku daljnu stranu, autor plaća 20 evra po strani.

UPUTSTVO AUTORIMA ZA TEHNIČKO SREĐIVANJE RADOVA

Rezime je poseban Word dokument, "ABSTRACT". Za domaće autore je dvojezičan (srpski i engleski). Inostranim autorima rezime se prevodi na srpski jezik besplatno.

Ovaj dokument treba da sadrži: 1) ime autora, zanimanje i zvanje, adresu prvog autora preko koje se obavlja sva potrebna korespondencija; 2) naslov rada; 3) kratak sažetak, do 100 reči, 4) do 5 ključnih reči

Rad je poseban fajl, „TEXT“ koji sadrži priloge i slike uključene u tekst. Na kraju rada nalazi se spisak literature i eventualno zahvalnost. Reference korišćene literature treba navesti u srednjim zagradama i grupisati ih na kraju rada po numeričkom redosledu.

Dužina rada:	Max 16 stranica B5 formata, ne uključujući rezime
Tekst procesor:	Microsoft Word
Margine:	levo/desno: mirror margine; unurašnja : 2.5; spoljna: 2 cm vrh: 2.5 cm, dno: 2 cm
Font:	Times New Roman, 10 pt
Naslov rada:	Velika slova, bold, 11 pt
Naslov poglavlja:	Velika slova, bold, 10 pt
Naslov podpoglavlja:	Mala slova, bold, 10 pt
Širina tabela, dijagrama:	max 125 mm
Nazivi slika, tabela:	Figure __ : Times New Roman, italic 10 pt Table _ : Times New Roman, italic 10 pt
Dostavljanje rada	Elektronski

E-mail: mvm@kg.ac.rs ; alex@kg.ac.rs ili poštom na adresu Časopisa

Redakcija časopisa M V M

Mašinski fakultet u Kragujevcu

Sestre Janjić 6, 34000 Kragujevac, Srbija

Po objavljivanju rada Redakcija časopisa šalje prvom autoru separat rada besplatno.

Autori uživaju popust 50% od pretplatne cene za tekuću godinu.

Mobility &

Motorna

Vehicle

**Volume 36
Number 2
June 2010.**

Vozila i

Mechanics

Motori

Ile Mircheski Tatjana Kandikjan Petar Simonovski	VIRTUAL TESTING AND EXPERIMENTAL VERIFICATION OF SEAT COMFORT IN DRIVER'S SEAT FOR PASSENGER AUTOMOBILE	7-20
Popa Dinel Parlac Sebastian Dejanu Marcel	THEORETICAL AND EXPERIMENTAL STUDY OF THE MECHANISMS USED IN THE CONSTRUCTION OF PLANETARY TRANSMISSION OF HYBRID CARS	21-36
Lilo Kunchev Nikolay Pavlov	COMPARATIVE ANALYSIS ON MATHEMATICAL MODELS DESCRIBING VIBRATIONS OF AUTOMOTIVE INDEPENDENT SUSPENSIONS	37-52
Catalin-Adrian Neacsu Mariana Ivanescu Ion Tabacu	NUMERICAL SIMULATION OF AIR FLOW THROUGH TWO DIFFERENT SHAPED AIR VENTS	53-65

Mobility &

Motorna

Vehicle

**Volume 36
Number 2
June 2010.**

Vozila i

Mechanics

Motori

Ile Mircheski Tatjana Kandikjan Petar Simonovski	VIRTUALNO ISPITIVANJE I EKSPERIMENTALNA VERIFIKACIJA UDOBNOSTI VOZAČEVOG SEDIŠTA ZA PUTNIČKE AUTOMOBILE	7-20
Popa Dinel Parlac Sebastian Dejanu Marcel	TEORIJSKO I EKSPERIMENTALNO PROUČAVANJE MEHANIZAMA KORIŠĆENIH U KONSTRUKCIJI PLANETARNIH PRENOSNIKA HIBRIDNIH VOZILA	21-36
Lilo Kunchev Nikolay Pavlov	UPOREDNA ANALIZA MATEMATIČKIH MODELA KOJI OPISUJU OSCILACIJE NEZAVISNIH SISTEMA ELASTIČNOG OSLANJANJA AUTOMOBILA	37-52
Catalin-Adrian Neacsu Mariana Ivanescu Ion Tabacu	NUMERIČKA SIMULACIJA PROTOKA VAZDUHA KROZ DVA VENTILACIONA OTVORA RAZLIČITOG OBLIKA	53-65

SUMMARIES REZIMEA

¹ VIRTUAL TESTING AND EXPERIMENTAL VERIFICATION OF SEAT COMFORT IN DRIVER'S SEAT FOR PASSENGER AUTOMOBILE

Ile Mircheski, Tatjana Kandikjan, Petar Simonovski, Ss Cyrill & Methodius University, Faculty of Mechanical Engineering, Karpos II - bb, 1000 Skopje, Republic of Macedonia

UDC: 629.014:656.052]:004.896
519.654:629.014

Abstract

In this paper, the effects of the thickness and density of polyurethane foam on the seating comfort in driver's seat for passenger automobile are presented. The comfort is estimated by analysis of the pressure distribution on the contact surface of the virtual human body and the seat cushion foam. The comfort seating posture for the virtual model of human in driver's seat is defined on the base of comfort angles. The virtual testing is performed with software package ABAQUS, which can simulate dynamic processes using FEA. The testing includes variation of the thickness and density of polyurethane foam and variation of the body sizes with 50th and 80th percentiles. The results from the virtual testing are confirmed experimentally with pressure distribution mapping sensors.

Key words: Seating comfort, comfort posture, virtual testing, virtual model of seat, virtual model of human, Finite element analysis (FEA).

VIRTUALNO ISPITIVANJE I EKSPERIMENTALNA VERIFIKACIJA UDOBNOSTI VOZAČEVOG SEDIŠTA ZA PUTNIČKE AUTOMOBILE

UDC: 629.014:656.052]:004.896
519.654:629.014

Rezime: U radu je prikazan uticaj debljine i gustine poliuretanske pene na udobnost vozačevog sedišta za putnički automobile. Udobnost je ocenjena analizom raspodele pritiska na kontaktnoj površini između virtualnog ljudskog tela i ispune jastuka sedišta. Udoban položaj pri sedenju kod virtualnog modela čoveka koji sedi na vozačevom sedištu definisan je na osnovu uglova udobnosti. Virtualno ispitivanje je izvršeno u softverskom paketu ABAQUS koji može da simulira dinamičke procese korišćenjem analize konačnim elementima. Ispitivanje uključuje variranje debljine i gustine poliuretanske pene i variranje

¹ Received: May 2010.
Accepted: June 2010.

Primljen: U Maju, 2010.god
Prihvaćen: U Junu, 2010.god.

veliĉine tela sa 50% i 80% modela. Rezultati virtualnih ispitivanja potvrđeni su eksperimentalno pomoću senzora za mapiranje raspodele pritiska.

Ključne reči: udobnost sedišta, udobni položaj, virtualno ispitivanje, virtualni model sedišta, virtualni model čoveka, analiza konaĉnim elementima.

VIRTUAL TESTING AND EXPERIMENTAL VERIFICATION OF SEAT COMFORT IN DRIVER'S SEAT FOR PASSENGER AUTOMOBILE

Ile Mircheski¹, Tatjana Kandikjan, Petar Simonovski

UDC: 629.014:656.052]:004.896

519.654:629.014

1. INTRODUCTION

The choice of passenger automobile depends on a lot of factors, such as, vehicle type, brand, trend, security, performance, space inside in the vehicle, design of the vehicle interior, additional equipment and other. Also, the seat comfort is very important issue where the owners of automobiles are very careful. Because the long time they spend in their car, people complain on pain caused by the discomfort of the seats. The expectations of customers regarding the seat comfort are continuously increasing.

The manufacturers of seats for passenger automobiles have to respond fast and appropriate on market requirements and offer quality and comfort seats. The manufacture of automobile seats, from the start of product development to the fabrication needs long time and lot of financial resources. The manufacturers of automobile seats make prototypes and test the comfort of their seats with aim to come to the desired results. By making few prototypes, the manufacturers lose a lot of time and financial costs. The vehicle process development is based on the virtual design of the vehicle structure and its verification, unlike from the past when the process development was based on the specific experience of the manufacturers of passenger automobiles. With help of the software for virtual modeling and representation of vehicle structure and the software which can simulate processes and system behavior, today the time needed for testing of physical prototypes is reduced. As a consequence, time and price for testing in obtaining of new or improved product is reduced. Lately, virtual testing of virtual models of automobile seats and virtual models of humans are applied in development of automobile seats.

The aim of this paper is to determine the influence on the construction parameters, such as the thickness and density of polyurethane foam, on the seating comfort for 50th and 80th percentile of man in the driver's seat for passenger automobile.

2. DEFINITION OF COMFORT SEATING ANGLES

The starting point of the process of vehicle design is the description on the people who have to be transported. In order to perform the overall dimensioning of the vehicle, sitting of the driver and other passengers, arrangement of all handling devices and controls, as well as application of all safety regulations and legislation, have to be considered. The design

¹ Corresponding author e-mail: ile_mirceski@mf.edu.mk, Phone: +389 2 3099 245, Ss Cyril & Methodius University, Faculty of Mechanical Engineering, Karpos II - bb, 1000 Skopje, Republic of Macedonia

process starts with the definition of a user population and with obtaining of human body data.

The area swept out by the movement of the hand can be used to describe ‘workspace envelopes’, zones of easy or maximum reach around an operator. The size and shape of the workspace envelope depends on the position of the human body. In case of driver’s work position in the vehicle, several functional measurements determine the important parameters of the comfort: the angels in elbow joint, shoulder joint, hip joint, knee joint, ankle joint and torso orientation (Figure 1).

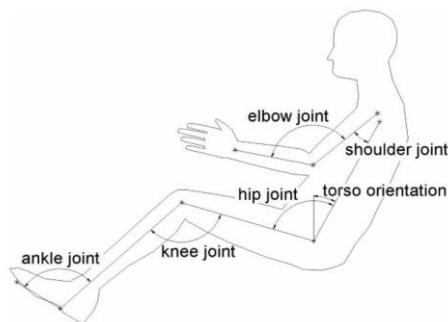


Figure 1: Parameters of driver’s work position [17]

In order to obtain the driving comfort, the parameters of driver’s position have to be always in the comfortable range [3]. Few researchers during the past few years have offered their recommendations about the ranges of comfortable angles [10]. There are big differences between their recommendations. Some of them recommend discrete comfort angles, and the others recommend ranges of comfort.

Using the fact that RAMSIS software [15] is specialized for the ergonomics in vehicles, we decided to adopt the recommended discrete comfort angles included in the incorporated RAMSIS data bases (Table 1). They will describe the driver’s seating posture for the following testing conditions.

Table 1: Adopted comfortable angles for the driver’s seating posture

Torso orientation	27 ⁰
Angle of shoulder joint	22 ⁰
Angle of elbow joint	127 ⁰
Angle of hip joint	99 ⁰
Angle of knee joint	119 ⁰
Angle of ankle joint	103 ⁰

In this paper, the research is performed with anthropometric types of 50th and 80th percentile of man. Because the seats are for urban passenger automobile, the analysis with 80th percentile of man is considered in order to encounter bigger population. Experiments for the

extreme case of population are not needed because their anthropometric measures are very big and the population is small. About 80% of all population will be covered with the analysis of anthropometric types of 80th percentile of man [1]. The analysis with 50th percentile of man is included for comparison of the results.

3. CREATING OF VIRTUAL MODEL OF HUMAN WITH CHARACTERISTICS OF BONES AND MUSCLES

Geometric data of virtual models of human are taken from the data base of the programming module Human Builder in Catia [5,9]. The virtual human model is composed of two parts, muscle tissue and skeleton. The human skin is not taken in the analysis because it is geometrically very complicated and has little impact on the results of the pressure distribution analysis [6]. The geometry of the skeleton is simplified with the aim to reduce the time needed for calculation of the numerical model with FEA, but the model should not be oversimplified because it will influence the validity of the received values from pressure distribution. Pelvis, femurs and simplified model of skeleton from virtual model of human are shown in the figure 2. The FEA model for numerical calculation is represented with the meshed model of the human with the characteristics of muscles tissue and bones. The mesh is created with tetrahedron elements, which are suitable for complicated geometric models.

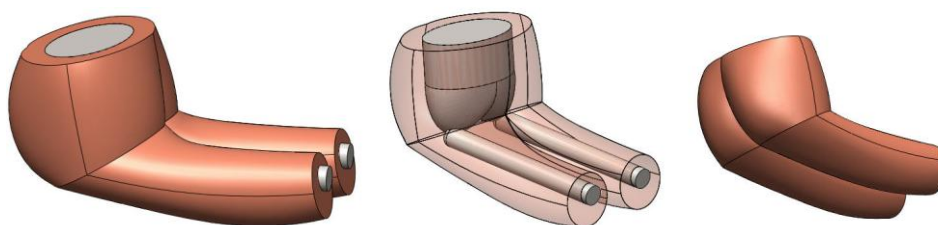


Figure 2: Geometrical representation of part of virtual model of human – pelvis, femurs and simplified muscle tissue

In figure 3, the mesh of human muscle tissue is composed of smaller finite elements than the mesh of simplified model of human skeleton. The human skeleton is not the goal of this analysis. The goal of the analysis is the human muscle tissue where the real contact with the seat occurs, and from where the values for pressure distribution are read.

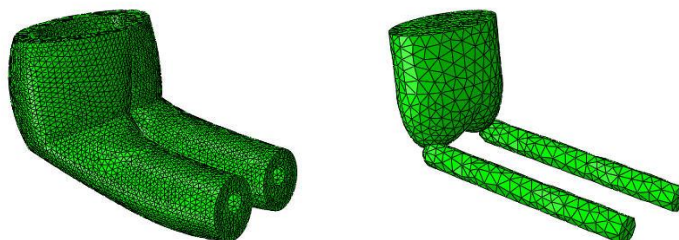


Figure 3: The FEA mesh model of the seating human

For human bone structures, the skeleton is assumed to be a rigid body. The human skeleton is a rigid body because the bones are not being deformed when the human body is in the seating position.

Few of the authors that worked with virtual testing of human muscle tissue are (E. Pennestri, P. P. Valentini, L. Vita [9]; A. Siefert, S. Pankoke, H. P. Wolfel [13]; and Verver, M [16]). The authors give different kinds of definition of the human muscle tissue. Verver, M [16] in her doctoral dissertation describes the parameters which define the non-linear mechanical behavior of human muscle tissue with the software package ABAQUS [2,4,7], with hyperelastic isotropic material model of Mooney – Rivlin. The strain energy function is defined by [16] as:

$$W = A_1(J_1 - 3) + A_2(J_2 - 3) + A_3(J_3^{-2} - 1) + A_4(J_3 - 1)^2 \quad (1)$$

where J_1 , J_2 and J_3 are the invariants of the right Cauchy-Green strain tensor. The right Cauchy-Green strain tensor is defined by [16]:

$$\underline{C} = \underline{F}^T \cdot \underline{F} \quad (2)$$

where \underline{F} is the deformation tensor. J_1 , J_2 and J_3 have been defined [16] as:

$$\begin{aligned} J_1 &= \text{trace}(\underline{C}) \\ J_2 &= \frac{1}{2} \left(\text{trace}^2(\underline{C}) - \text{trace}(\underline{C})^2 \right) \\ J_3 &= \det(\underline{C}) \end{aligned} \quad (3)$$

The second Piola-Kirchhoff stress tensor is obtained by differentiating the strain energy function W with respect to the right Cauchy-Green strain tensor [16]:

$$\underline{S} = 2 \frac{\partial W}{\partial \underline{C}} \quad (4)$$

The material parameters A_3 and A_4 are function of the coefficients A_1 and A_2 :

$$A_3 = \frac{1}{2} A_1 + A_2 \quad \text{and} \quad A_4 = \frac{A_1(5\nu - 2) + A_2(11\nu - 5)}{2(1 - 2\nu)} \quad (5)$$

The values for A_1 , A_2 and ν have been set to: $A_1 = 0.00165 \text{ MPa}$, $A_2 = 0.00335 \text{ MPa}$ и $\nu = 0.49$. These values for material parameters are used by Verver, M [16].

The value for density of human muscle tissue is defined with volume and body mass. The density of human muscle tissue is $0,0026 \text{ kg/m}^3$.

4. CREATION OF THE VIRTUAL MODEL OF DRIVER'S SEAT CUSHION WITH CHARACTERISTICS OF THE USED MATERIALS

The driver's seat for passenger automobile consists mainly of three parts: seat cushion, seat back and head restraint [8]. In the figure 4, the seat cushion assembly is represented with the sheet metal holder and the polyurethane foam. The polyurethane foam from the seat cushion is placed on the sheet metal holder. The sheet metal is with thickness of 1 mm and is supported by the seat mechanical structure on four small perpendicular support area.



Figure 4: Sheet metal holder, the foam from seat cushion

The driver's seat cushion for the driver's seat, shown in figure 4, is made by Johnson Controls. The geometrical data are used for the analysis of the influence of the thickness and density of the polyurethane foam on the seating comfort.

The investigation begins with a virtual model of the seat cushion which is the same with the real seat, shown in figure 4. The virtual model of the seat cushion in figure 4 is shown in figure 5. In figure 5 we can see also two elliptical holes, which have a significant influence on the seat comfort. In the figure 6, the dimensions of the seat cushion are shown.

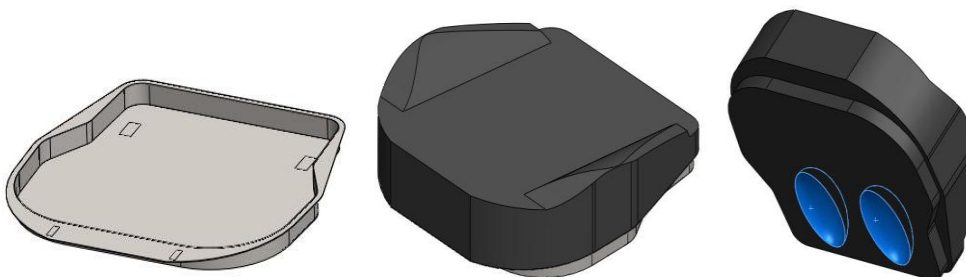


Figure 5: Virtual model of seat cushion

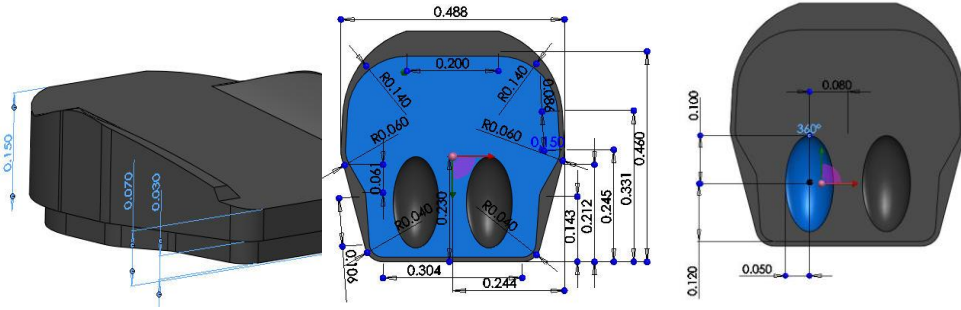


Figure 6: Dimensions of the seat cushion

The meshed model with tetrahedron elements is prepared to be used in FEA. The meshed model of the seat cushion, which corresponds to the virtual model of the seat in figure 5 is shown in figure 7.

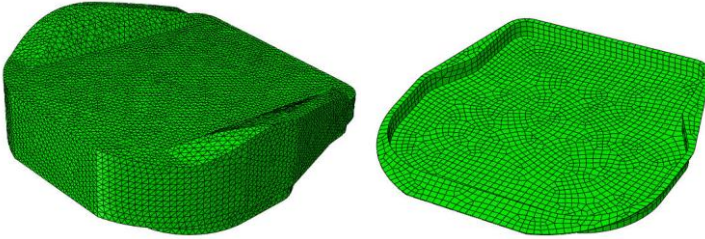


Figure 7: The meshed model of seat cushion

As means for the description of foam materials in ABAQUS [2,4,7,11], a hyper-elastic law is used. The elasticity of the material is described via the potential energy U of elastic deformation. The applied potential function for foams (Eq. (6)) considers nearly full compressibility of polyurethane foams.

Strain energy potential of compressive foams is computed as Ogen funcion:

$$U = \sum_{i=1}^N \frac{2\mu_i}{\alpha_i^2} \left[(\lambda_1^{\alpha_i} + \lambda_2^{\alpha_i} + \lambda_3^{\alpha_i} - 3) + \frac{1}{\beta_i} (J^{-\alpha_i \beta_i} - 1) \right] \quad (6)$$

The potential energy U is defined by the following parameters: μ_i are the coefficients of initial shear modulus, λ_{1-3} the principal stretches, α_i the standard material parameter, β_i the coefficients for degree of compressibility and J the elastic volume ratio. The free material parameters μ_i , α_i and β_i are determined experimentally, with the average values out of loading and unloading.

With bold line in figure 8, are represented the nonlinear characteristic of polyurethane foam which is described with Ogden function with $N = 1$, $\mu = 10kPa$, $\alpha = 8$ and Ogden function with $N = 2$, $\alpha_1 = 17,4$, $\mu_1 = 18,3kPa$, $\alpha_2 = -2,0$, $\mu_2 = 0,21kPa$ and Poisson ratio $\nu = 0$ [12].

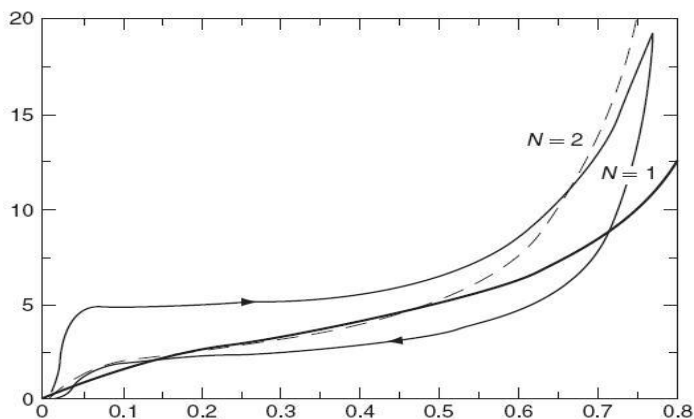


Figure 8: Nonlinear characteristic for flexible polyurethane foam [12]

Ogden function from second degree with $N = 2$ is used for description of nonlinear behavior of flexible polyurethane foam [14].

The density of polyurethane foam is given from the manufacturer Johnson Controls Inc. and is 50 kg/m^3 .

5. EXPERIMENTAL TESTING AND VIRTUAL TESTING OF THE MODEL

5.1. Measurement equipment

For obtaining of pressure distribution in the contact surface between the driver's seat and the driver the equipment from manufacturer XSENSOR Technology Corporation is used. The measurement equipment consist of few elements such as: sensor platform X3 PRO, sensor pad for measuring of pressure distribution, Mini – B USB cable, 12 VDC 3.75 A AC/DC power supplier, electronic for connection of sensor pad and PC, X3 node, PC and software XSENSOR - X3 MEDICAL v6.0 used for data acquisition. The sensor pad is of type PX100:36.36.02 composed of a seat sensor with resolution of 1296 sensible points, with excellent flexibility and endurance. The measurement pressure range is between 10 – 200 mmHg. The resolution of pressure measurement is 1,27 cm. The elements which are included in the measurement equipment for measuring of pressure distribution between two bodies in contact are shown in figure 9.



Figure 9: XSENSOR - X3 PRO system for measuring of pressure distribution

5.2. The results from the experimental measuring and virtual testing

For measuring of the pressure distribution between the driver’s seat cushion from passenger automobile and the man, we use the seat described in figure 4. The measuring is performed with men from 50th and 80th percentile. The human weight of 50th percentile man before the testing was 71 kg and for 80th percentile man was 78,5 kg. The measured weights are the same with the weights of the corresponding virtual models. Before the measuring the participants were seated according to the comfort angles. The measured pressure distribution and the values for maximum contact pressure are shown in figure 10.

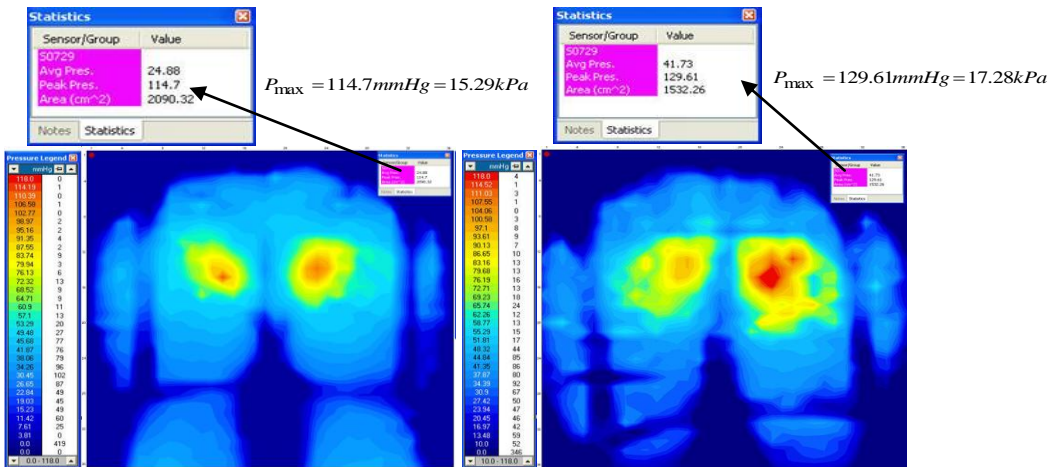


Figure 10: Pressure distribution between seat cushion and participants from 50th and 80th percentile

The boundary conditions in the simulation are defined on the seat geometry. In reality, the seat is fixed from below on four supports (in precisely defined areas) located on the sheet mental. The fixing is defined with translations and rotations equal to zero.

The initial conditions in the simulation is defined for the time $t = 0$ s. In the initial moment of the simulation, the virtual model of the human is placed above the seat without a contact between them, and the initial speed is set to 0.

The loading condition in the simulation is defined with gravity of 9810 mm/s^2 .

The contact between the virtual model of human and the seat cushion is defined with selecting of surfaces that come in contact. In reality, there is friction between contact surfaces. The coefficient of friction between contact surfaces is 0.75. The coefficient of friction is obtained experimentally [12].

The pressure distributions on the seat contact surface resulting from the analyses for 50th (left) and 80th (right) percentile are shown in figure 11.

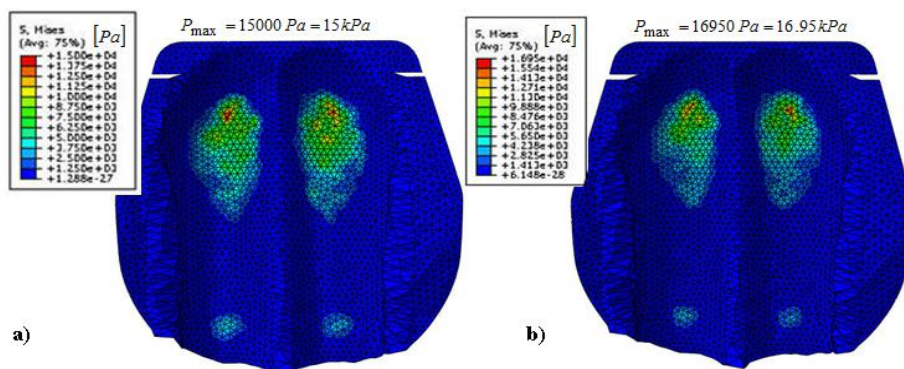


Figure 11: Pressure distribution on the contact surface of virtual seat cushion and virtual model of human from; a) 50th and b) 80th percentile

The experimental values of the maximum contact pressure in the contact surface between the seat cushion and the human are given in table 2. The measured values are close to the values obtained from the virtual testing.

Table 2: Values for maximum contact pressure

Human percentile	Maximum contact pressure from experimental measurement [kPa]	Maximum contact pressure from virtual testing [kPa]
50-tile	15,29	15,00
80 -tile	17,28	16,95

The human skin and seat cover are not considered in the virtual testing. For this reason, there is a difference in the results obtained from the experiment and the virtual testing of

about 2%. This difference is small and approves the use of the virtual model instead of the experimental testing of seat prototypes.

6. INFLUENCE OF THICKNESS AND DENSITY OF POLYURETHANE FOAM ON THE SEATING COMFORT

According to the data found in literature [12], comfortable seats are seats with maximum contact pressure less from 12 *kPa*.

For the seat geometry shown in the figure 5, the influence of the foam thickness on the maximum contact pressure is examined using the virtual models of the seat and human from 50th and 80th percentile. The initial seat has foam thickness of 70 mm. If the foam thickness is reduced to 60 mm, 50 mm, and 40 mm, than the contact preasure increases, first slowly and than rapidly, such as shown in figure 12.

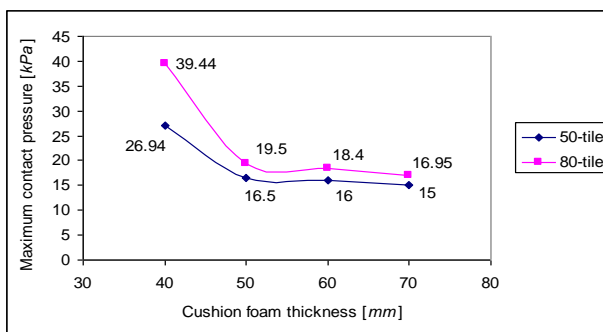


Figure 12: Relationship of maximum contact pressure and seat cushion thickness

To examine the influence of the dencilty of the polyurethane foam on the contact preasure, six virtual testings for design shown in the figure 5 are performed with the foam thickness of 70 mm. The results obtained from virtual testing of six virtual models of seats with density of 30 *kg/m³*, 40 *kg/m³* and 50 *kg/m³* and two types of virtual models of human from 50th and 80th percentile are shown in figure 13.

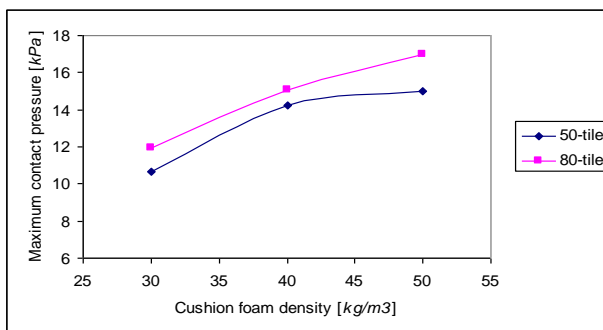


Figure 13: Relationship of maximum contact pressure and density of the polyurethane foam

7. CONCLUSIONS

The virtual testing of seating process in driver's seat for passenger automobile allows fast and simplified review of the phenomena that occur during the seating. This virtual testbench provides a mechanism for investigation of new design ideas for new types of seats. Using this virtual testbench, the new design of seat can be validated in the product development phase, thus avoiding the financial costs and saving time for making physical prototypes.

The influence thickness of the seat cushion foam on the maximum contact pressure is examined. From the diagram shown in the figure 12, it is obvious that with reducing of the foam thickness below certain limit value, the seating comfort is deteriorating gradually.

The foam density has an important influence of the value of the maximum contact pressure. As shown in figure 13, with reducing of the foam density the value of the maximum contact pressure is decreasing slowly, and with that the seating comfort is improving.

REFERENCES

- [1] Attwood D. A., Deeb J. M., Danz-Reece M. E.: "Ergonomic Solutions for the Process Industries", Vol. 1, 2004, Elsevier Inc.
- [2] ABAQUS Example Problems Manual, 2008, ABAQUS, Inc.
- [3] Bernaer, J. D.: "Ergonomic for beginners", Second Edition, 2001.
- [4] CATIA V5 Tutorial, 2008, SIMULTIA, Inc.
- [5] Dickson, S.: "CATIA V5 Design with Analysis", 2007, The Hong Kong Polytechnic University.
- [6] Ebe, K., Griffin, J. M.: "Factors affecting static seat cushion comfort", 2001, Taylor and Francis.
- [7] Getting Started with ABAQUS/Standard, 2008, ABAQUS, Inc.
- [8] Kandikjan, T.: "Engineering Design and CAD", 2006, Faculty for Mechanical Engineering, Skopje.
- [9] Karam, F., Kleismit, C.: "CATIA V5", 2006, SDC Publications.
- [10] Kroemer, K.H.E.: "Extra – ordinary" Ergonomics", Vol. 1, Taylor and Francis, 2006.
- [11] Liu, G. R., Quek, S. S.: "The Finite Element Method: A Practical Course with Abaqus", Department of Mechanical Engineering, 2003, National University of Singapore.
- [12] Nigel, J. M.: "Polymer Foams Handbook: Engineering and Biomechanics Applications and Design Guide", 2007, Butterworth-Heinemann.
- [13] Siefert, A., Pankoke, S., Wolfel, H. P.: "Virtual optimization of car passenger seats: Simulation of static and dynamic effects on driver' seating comfort", International Journal of Industrial Ergonomics, Vol. 38, 2008, Science Direct, pages 410-424.
- [14] Spyarakos, C. C., Raftoyiannis, J.: "Linear and Nonlinear Finite Element Analysis In Engineering Practice", 1997, Algor Inc.
- [15] Van der Meulen, P., Seidl, A.: "Ramsis – The Leading Cad Tool for Ergonomic Analysis of Vehicles", Human Solutions GmbH, Europaallee 10, 67657 Kaiserslautern, Germany.

- [16] Verver, M. M.: "Numerical tools for comfort analysis of automotive seating", Dissertation, 2004, Technische Universiteit Eindhoven.
- [17] Vogt, C., Mergl, C., Bubb, H.: "Interior Layout Design of Passenger Vehicles with RAMSIS", *Human Factors and Ergonomics in Manufacturing*, Vol. 15, No. (2), 2005, Wiley Periodicals, Inc., pages 197-212.

SUMMARIES
REZIMEA

**¹ THEORETICAL AND EXPERIMENTAL STUDY OF THE
MECHANISMS USED IN THE CONSTRUCTION OF PLANETARY
TRANSMISSION OF HYBRID CARS**

Popa Dinel, Parlac Sebastian, University of Pitesti, Romania
Dejanu Marcel, Muntenia Invest S.A. Bucharest, Pitesti, Romania

UDC: 519.872:001.895]:629.113

Abstract

This paper presents theoretical and experimental results obtained from the use of planetary mechanisms with two degrees of mobility coupled thermal and electric power sources. These mechanisms are frequently used in hybrid cars transmissions with an series-parallel architecture (full hybrid). After presenting the experimental mechanisms and the system of differential equations of motion there is a theoretical study on stability of motion.

Differential equations of motion are obtained using Lagrange equations and the stability of the motion is always studied. Numerical data necessary to the theoretical study were obtained by modeling the mechanism elements in a CAD software where, after the presentation, resulted their mechanical and geometric properties. At the end of the paper is presented the stand in order to obtain experimental data, the measuring chains and the results.

Key words: power source, hybrid drive, equations of motion, stability of motion, experimental determinations.

**TEORIJSKO I EKSPERIMENTALNO PROUČAVANJE MEHANIZAMA
KORIŠĆENIH U KONSTRUKCIJI PLANETARNIH PRENOSNIKA
HIBRIDNIH VOZILA**

UDC: 519.872:001.895]:629.113

Rezime: Ovaj rad prikazuje teorijske i eksperimentalne rezultate dobijene korišćenjem planetarnih mehanizama sa dva stepena slobode sa vezanim izvorima toplotne i električne energije. Ovi mehanizmi se često koriste u transmisijama snage hibridnih vozila sa redno-

¹ Received: May 2010.
Accepted: June 2010.

Primljen: U Maju, 2010.god
Prihvaćen: U Junu, 2010.god.

paralelnom arhitekturom („full hybrid“). Nakon predstavljanja eksperimentalnih mehanizama i sistema diferencijalnih jednačina kretanja, prikazano je teorijsko istraživanje stabilnosti kretanja.

Diferencijalne jednačine kretanja su dobijene korišćenje Lagrange-ovih jednačina, pri čemu je uvek proučavana stabilnost kretanja. Numerički podaci neophodni za teorijska izučavanja dobijeni su modeliranjem elemenata mehanizama u CAD softveru, u kome su, nakon prikazivanja, proizašle kao rezultat mehaničke i geometrijske karakteristike. Na kraju rada prikazani su probni sto za dobijanje eksperimentalnih podataka, merni lanci i rezultati.

Ključne reči: izvor energije, hibridni pogon, jednačine kretanja, stabilnost kretanja, eksperimentalno određivanje

THEORETICAL AND EXPERIMENTAL STUDY OF THE MECHANISMS USED IN THE CONSTRUCTION OF PLANETARY TRANSMISSION OF HYBRID CARS

Popa Dinel¹, Parlac Sebastian, University of Pitesti, Romania

Dejanu Marcel, Muntenia Invest S.A. Bucharest, Pitesti, Romania

UDC: 519.872:001.895]:629.113

INTRODUCTION

The necessity of protecting the environment by limiting and controlling the gas emissions that contributes considerably to the greenhouse effect, by limiting the excessive fuel consumption from the limited fossil fuel reserves needs a new orientation to new technologies for powering future vehicles.

A promising solution on medium term is that of hybrid propulsion. This idea is in the attention of the researchers from the largest firms that are producing automobiles and also of the research centers.

The hybrid drive systems used at automobiles are systems where the energy required for self-propulsion is provided at least by two sources based on different principles of generating energy. The general components of a hybrid drive system are:

- a transformer of irreversible energy,
- a stocking system of reversible energy,
- a reversible coupling system.

The coupling system has the role of ensuring the energy transformation between the driving wheels and the other two components. It can be made:

- through an irreversible connection between the energy transformer and the driving wheels that make possible the self propulsion of the vehicle;
- through a reversible connection between the battery and the wheels, that is used for the self propulsion of the vehicle or for the recovery of the breaking energy;
- through an irreversible connection between the energy transformer and the battery that is used for recharge when the vehicle stops.

The Japanese constructors were the first who introduced hybrid vehicles in production. The THS (Toyota Hybrid System), is a solution that joins both electric and heat engine traction system. Coupling both thermal and electrical power is made by a planetary mechanism.

¹ Corresponding author e-mail: dinel_popa@yahoo.com, University of Pitesti, Romania

THE STUDY OF PLANETARY MECHANISMS USED IN POWER SOURCES CONNECTIONS

KINEMATIC SCHEME

Two planetary mechanisms that can be used in transmitting power to a vehicle wheels are presented in figure 1. The hybrid auto-propulsion of the automobiles is made with a heat engine (MT) and an electrical engine (ME) that is powered from a battery with an accumulator (BA) of high voltage.

The accumulator battery is charged even during the displacement of the automobile because of an electric generator (GE) driven by the heat engine. The power sources (the heat engine, the electric generator, the electrical engine) can be coupled by the planetary mechanism with two degrees of loose (fig. 1 with a double satellite with external gearing or with a simple satellite with internal gearing (fig. 1, b). The mechanism from figure 1 b, is used in the construction of hybrid transmission for the hybrid vehicles Toyota Prius and Lexus.

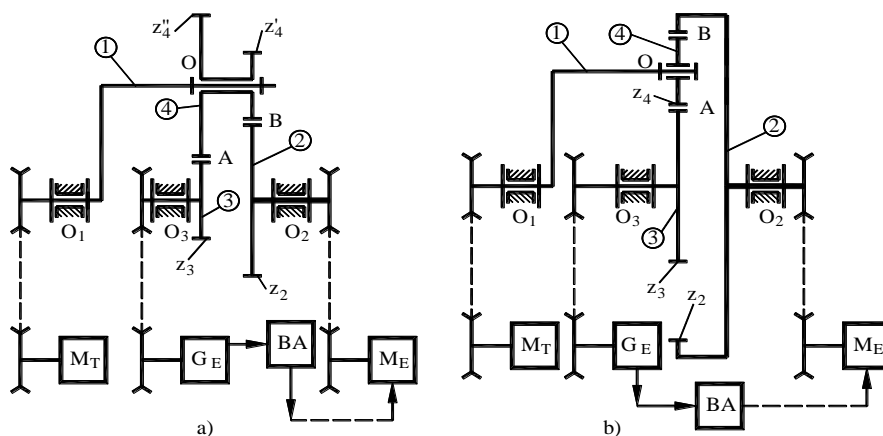


Figure 1: Planetary mechanisms

NOTATIONS

It is considered the coupling system from figure 1, a and the notations:

- J_i , $i = 1, 2, 3, 4$, axial moments of inertia of the elements marked with 1, 2, 3, 4;
- m_4 , weight of the satellites 4;
- R_4 , the length of the planetary carrier 1;
- z_2, z_3, z_4, z_4'' the number of teeth of the tooth wheels;
- i_1, i - the equations defined by the relations

$$i_1 = \frac{z_2}{z_4}; i = \frac{z_2 z_4}{z_3 z_4} \quad (1)$$

- A, B, C , parameters - inertial parameters defined by the relations

$$\begin{aligned} A &= J_1 + m_4 R^2 + (1 + i_1^2) J_4 + (1 - i) J_3 \\ B &= -(1 - i) i J_3 + J_4 (1 + i_1) i_1 \\ C &= J_2 + J_3 i^2 + J_4 i_1^2 \end{aligned} \quad (2)$$

- $\theta_1, \theta_2, \theta_3$ the rotation angles of the elements 1, 2, 3,
- $\omega_1, \omega_2, \omega_3, \omega_4$ - the absolute angular velocities of the elements 1, 2, 3, 4,
- M_1, M_2, M_3 moments that act on the elements 1, 2, 3,

If the mechanisms 1, b are used then the modifications that are made are:

$$i_1 = -\frac{z_2}{z_4}; i = -\frac{z_2}{z_3} \quad (3)$$

and all the other notations remain the same.

THE KINETIC ENERGY AND THE GENERALIZED FORCES

Using the Wills method for the mechanism from figure 1 a, these relations are obtained

$$\frac{\omega_4 - \omega_1}{\omega_2 - \omega_1} = -\frac{z_2}{z_4}; \frac{\omega_3 - \omega_1}{\omega_4 - \omega_1} = -\frac{z_4}{z_3} \quad (4)$$

From which, with the notations (1) we deduct the equalities:

$$\begin{aligned} \omega_3 &= \omega_1(1 - i) + \omega_2 i \\ \omega_4 &= \omega_1(1 + i_1) + \omega_2 i_1 \end{aligned} \quad (5)$$

that are still available for the mechanism from figure 1, b is replaced with i_1 cu $-i_1$ and i cu $-i$. The kinetic energy of the system:

$$E_C = \frac{1}{2}(J_1\omega_1^2 + m_4R^2\omega_1^2 + J_2\omega_2^2 + J_3\omega_3^2 + J_4\omega_4^2) \quad (6)$$

with the notations (2) and (5) the equation becomes:

$$E_C = \frac{1}{2}(A\dot{\theta}_1^2 - 2B\dot{\theta}_1\dot{\theta}_2 + C\dot{\theta}_2^2) \quad (7)$$

The mechanic power at a certain time is given by:

$$P = M_1\omega_1 + M_2\omega_2 + M_3\omega_3 \quad (8)$$

or on the basis of the other relation (5)

$$P = [M_1 + M_3(1-i)]\omega_1 + (M_2 + M_3i)\omega_2 \quad (9)$$

and from here we deduct the generalized equations:

$$Q_1 = M_1 + M_3(1-i); \quad Q_2 = M_2 + M_3i. \quad (10)$$

DIFFERENTIAL EQUATIONS

Knowing the fact that:

$$\omega_1 = \dot{\theta}_1; \quad \omega_2 = \dot{\theta}_2 \quad (11)$$

and using the Lagrange equations

$$\frac{d}{dt} \left(\frac{\partial E_C}{\partial \dot{\theta}_i} \right) - \frac{\partial E_C}{\partial \theta_i} = Q_i, \quad i = 1, 2 \quad (12)$$

we obtain the differential equations

$$A\dot{\omega}_1 - B\dot{\omega}_2 = M_1 + M_3(1-i); \quad -B\dot{\omega}_1 + C\dot{\omega}_2 = M_2 + M_3i \quad (13)$$

or

$$\dot{\omega}_1 = \frac{[M_1 + M_3(1-i)]C + (M_2 + M_3i)B}{AC - B^2}; \quad \dot{\omega}_2 = \frac{[M_1 - M_3(1-i)]B + (M_2 + M_3i)A}{AC - B^2} \quad (14)$$

THE MOVEMENT STUDY IN PERMANENT REGIME

The permanent movement is deduced from the conditions:

$$\omega_1 = 0; \omega_2 = 0 \quad (15)$$

which goes to this equations:

$$\begin{aligned} [M_1 + M_3(1-i)]C + (M_2 + M_3i)B &= 0; \\ [M_1 + M_3(1-i)]B + (M_2 + M_3i)A &= 0 \end{aligned} \quad (16)$$

From the relations (16) is obtained the condition:

$$AC - B^2 > 0 \quad (17)$$

and then the equations (16) become:

$$M_1 + M_3(1-i) = 0; M_2 + M_3i = 0 \quad (18)$$

The sources of power are present by the characteristics movement-angular speed through the relations $M_i = M_i(\omega_i)$ and goes to the values: ω_1^* , ω_2^* , ω_3^* of the angular velocities and there are obtained the permanent conditions, deduced from the equation system:

$$\begin{aligned} M_1(\omega_1^*) + (1-i)M_3(\omega_3^*) &= 0; M_2(\omega_2^*) + iM_3(\omega_3^*) = 0; \\ \omega_3^* &= (1-i)\omega_1^* + i\omega_2^* \end{aligned} \quad (19)$$

If these values $M_2(\omega_2^*)$, $M_3(\omega_3^*)$ are related to the value of the moment $M_1(\omega_1^*)$ of the heat engine, the following relations are obtained:

$$\frac{M_2(\omega_2^*)}{M_1(\omega_1^*)} = -\frac{i}{i-1}; \quad \frac{M_3(\omega_3^*)}{M_1(\omega_1^*)} = -\frac{1}{i-1} \quad (20)$$

with the graphic representation from figure 2 and figure 3.

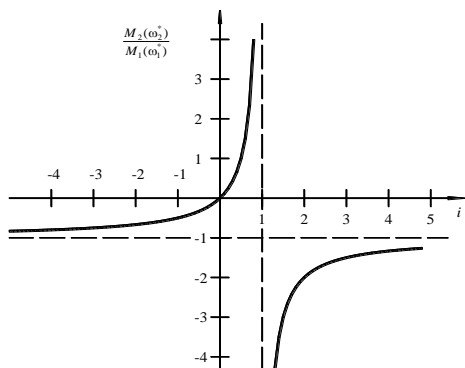


Figure 2: Graphic $\frac{M_2(\omega_2^*)}{M_1(\omega_1^*)} = -\frac{i}{i-1}$

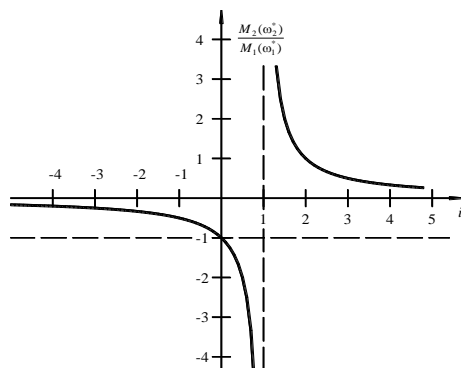


Figure 3: Graphic $\frac{M_3(\omega_3^*)}{M_1(\omega_1^*)} = -\frac{1}{i-1}$

The last relation (20) is represented in figure 4 for $i < 0$ and in figure 5 for $i > 1$.

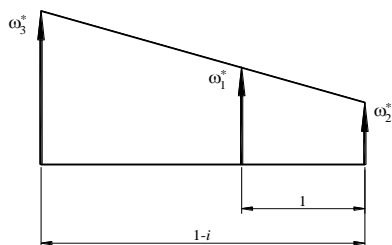


Figure 4: Representation of the relation $i < 0$

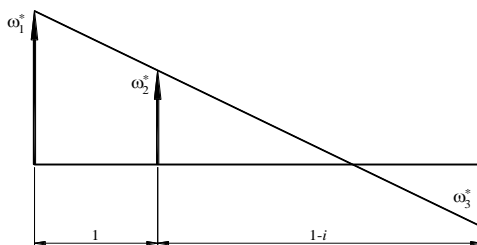


Figure 5: Representation of the relation $i > 1$

Starting from the supposition that the power of the engine $P = M_1\omega_1$ $P = M_1\omega_1$ is distributed to the generator and to the wheels sliding, it results that:

$$P_2 = M_2\omega_2 < 0; P_3 = M_3\omega_3 < 0 \tag{21}$$

$$P = |P_2| + |P_3| \tag{22}$$

and if it is admitted that $M_2 < 0$ then from figure 2 and 4 results that:

$$i < 0 \text{ or } i > 1 \tag{23}$$

If $i < 0$ results from figure 4 that $\omega_3^* > 0$ and from figure 2 that $M_3 < 0$ and because of that the value of P_2, P_3 is negative which means that the conditions (22) are respected.

If $i > 1$ from figure 4 results that $M_3 > 0$ and to respect the condition (22) is necessary that $\omega_3^* < 0$ (fig. 5) and:

$$\frac{\omega_2^*}{\omega_1^*} < \frac{i-1}{i} \quad (24)$$

Analogue is made for $i < 0$ and the complementary relation is obtained:

$$\frac{\omega_2^*}{\omega_1^*} > \frac{i-1}{i} \quad (25)$$

We can take into consideration at least two particular cases:

1. The heat engine works for charging the battery and the automobile is stopped ($\omega_2^* = 0$).

Results ($i > 1$) and

$$\omega_3^* = -(i-1)\omega_1^* < 0 \quad (26)$$

and how $M_3(\omega_3^*) > 0$ (fig. 4) the systems functionality is normal, the power consumed by the generator is equal with the power given by the heat engine.

2. Starting the electrical engine first and then the heat engine move the automobile.

In the first faze $\omega_1 = 0$ and for $i > 1$ results that:

$$\omega_3^* = i\omega_2^* > 0 \quad (27)$$

Considering that the angular velocity to wheel, the wheel being operated by the electrical engine, has the same way as the angular velocity of the generator, then the moment M_3 at the generator is negative. Next, by starting the heat engine, we reached to the situation from figure 5 where $\omega_3 < 0$ and $M_3 > 0$.

THE MOVEMENTS STABILITY

The solution ω_1^* , ω_2^* , ω_3^* is obtained from the (19) system and is stable even if $\Omega_i = \omega_i - \omega_i^*$, $i = 1, 2, 3$ are going through zero. In this way it will be studied the stability after the first approximation. There are obtained the linear approximations:

$$\begin{aligned}
 M_1(\omega_1^* + \Omega_1) &= M_1(\omega_1^*) + \Omega_1 M_{1p}(\omega_1^*); \\
 M_2(\omega_2^* + \Omega_2) &= M_2(\omega_2^*) + \Omega_2 M_{2p}(\omega_2^*); \\
 M_3(\omega_3^* + \Omega_3) &= M_3(\omega_3^*) + \Omega_3 M_{3p}(\omega_3^*)
 \end{aligned}
 \tag{28}$$

where by M_{ip} were denoted the functions derivatives $M_i(\omega_i^*)$.

By replacing the equations (14) and taking into account the notations:

$$\begin{aligned}
 \alpha &= \frac{1}{AC - B^2} \left[M_{1p}(\omega_1^*) + (1-i)^2 M_{3p}(\omega_3^*) \right]; \\
 \beta &= \frac{i(1-i)}{AC - B^2} M_{3p}(\omega_3^*); \quad \gamma = \frac{1}{AC - B^2} \left[M_{2p}(\omega_2^*) + i^2 M_{3p}(\omega_3^*) \right]
 \end{aligned}
 \tag{29}$$

it is obtained the linear system of differential equations:

$$\dot{\Omega}_1 = (\alpha C + \beta B)\Omega_1 + (\beta C + \gamma B)\Omega_2; \quad \dot{\Omega}_2 = (\alpha B + \beta A)\Omega_1 + (\beta B + \gamma A)\Omega_2
 \tag{30}$$

The characteristic equation becomes:

$$\begin{vmatrix}
 \alpha C + \beta B - r & \beta C + \gamma B \\
 \alpha B + \beta A & \beta B + \gamma A - r
 \end{vmatrix} = 0
 \tag{31}$$

or

$$r^2 + Dr + E = 0
 \tag{32}$$

where

$$D = -(\alpha C + 2\beta B + \gamma A); \quad E = (\alpha C + \beta B)(\beta B + \gamma A) - (\alpha B + \beta A)(\beta C + \gamma B)
 \tag{33}$$

By making the calculations, the following results are obtained

$$D = -\frac{1}{AC - B^2} \left\{ CM_{1p}(\omega_1^*) + AM_{2p}(\omega_2^*) + \left[i^2 A + 2i(1-i)B + (1-i)^2 C \right] M_{3p} \right\}$$

$$E = \frac{1}{AC - B^2} \left[M_{1p}(\omega_1^*) M_{2p}(\omega_2^*) + (1-i)^2 M_{2p}(\omega_2^*) M_{2p}(\omega_2^*) + i^2 M_{1p} M_{3p} \right] \quad (34)$$

For making the signs of the parameters D , E , there are taken into account the inequalities:

$$A > 0; C > 0; AC - B^2 > 0;$$

$$i^2 A + 2i(1-i)B + (1-i)^2 C > 0 \quad (35)$$

that are deduced from the element calculations from relation (2).

So, if $M_{ip}(\omega_i^*)$, $i=1, 2, 3$ are negative, then $D > 0$; $E > 0$, the equation (32) has real negative solutions or complex solutions with the real part negative and then the movement is a stable one.

The movement is unstable in the cases:

$$D > 0; E < 0, \quad D < 0; E > 0, \quad D < 0; E < 0 \quad (36)$$

THE CONSTRUCTIVE SOLUTION OF THE PROTOTYPE

The prototype has a mechanism constituted of a planetary mechanism with a double satellite (fig. 1, a) for coupling one heat engine and two electrical cars: a phase induction motor and an alternator.

The powers of the three engines is a result of a self-propulsion calculation of a vehicle with the performances: weight 600 kg, useful mass 200 kg, maximum speed 110 km/h, aerodynamic coefficient 0,3, rolling resistance 0,015 and frontal area of 2,56 m². So the calculus resulted:

- the power of the heat engine: 15,3 kW la 3600 rot/min,
- the power of the electric engine: 7,5 kW la 3000 rot/min,
- the power of the electric generator: 6 kW la 8000 rot/min.

For obtaining compact mechanical solutions we have used a heat engine fully equipped, air cooled and a three-phased engine with outputs on both sides like in figure 6.

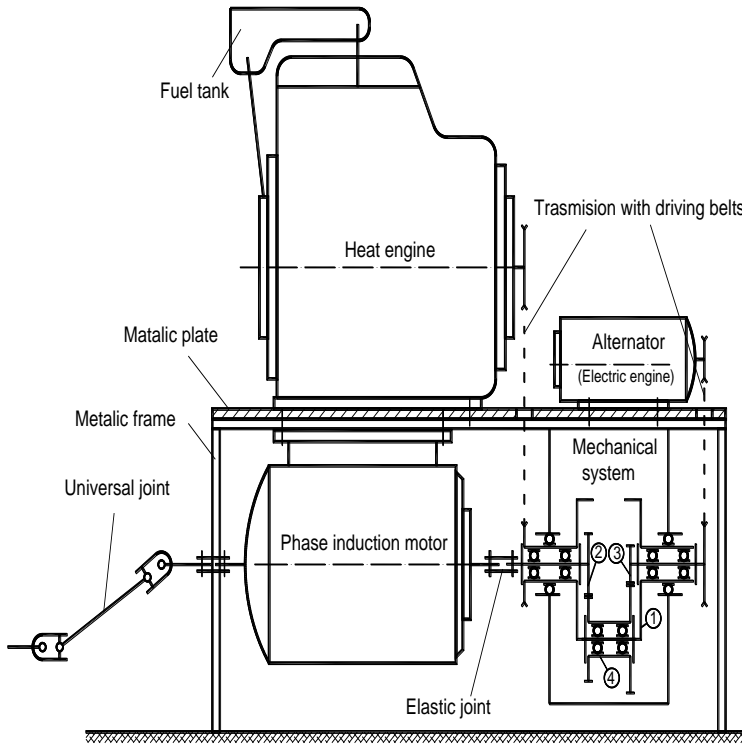


Figure 6: The constructive scheme of the prototype

In the same way the heat engine (MT from figure 1) will be located on the assembly: electric motor - mechanical system (ME – SM from figure 1).

The heat engine is coupled with the mechanical system using a transmission with driving belts, by separating the heat engine from the vibrations regarding the other parts of the mechanical system. Mechanically, the heat engine shaft is jointly in rotation with the port-satellite planetary arm mechanism.

The tooth wheels of the mechanical system have the following number of teeth: $z_3 = 20$ teeth, $z_2 = 35$ teeth, $z'_4 = 30$ teeth and $z''_4 = 45$ teeth. According to relation (1) the following values will result:

$$i = \frac{z_2 z''_4}{z_3 z'_4} = \frac{35 \cdot 45}{20 \cdot 30} = 2,625 \quad \text{and} \quad i_1 = \frac{z_2}{z_4} = 1,166$$

The electric generator (GE from figure 1) is a high power alternator or two alternators of medium power that are belt driven by the toothed wheel shaft joint (2). The generator is mounted in the upper part of the ensemble, on the same side with the heat engine.

The tensions of the two alternators are adjusted with two voltage relays, each alternator having its own accumulator battery. Next, the tensions of the two batteries are going to the consumers or to an inverter module that transforms alternative voltage into a three-phased direct current. There was never used such a module, three-phased voltage being available in the electric network of the test laboratory.

With the current configuration, where the generator is an alternator, an electric starter is necessary for the heat engine because the alternator isn't electric reversible.

In the circuit of a battery the commanding system of the electric starter of the heat engine was also introduced.

The elements of the mechanism were designed and modeled in AutoCAD and in CATIA V5 environments, being also checked in terms of mechanical stresses in CATIA and LS-Dyna.

There were obtained numerical models and there was established a loading program in five phases.

AutoCAD modeling of all components of the mechanical system has a main advantage of simplifying the process of determining the mechanical sizes and the inertia of the components and ensembles. A second advantage is that of transferring the modules to the software specialized in the analysis of stresses and tensions.

Modeling the elements let to the determination of the mechanism constants, given by the relations (2):

$$A = 0,00689117, B = 0,1110185 \text{ and } C = 0,0760352.$$

The differences appear between the sizes determined in AutoCAD and those experimentally obtained (weights, experimental determination of the inertia moments etc.) and are caused by not respecting the processing technology, the AutoCAD modeling being made with increased accuracy.

Modeling tooth wheels in AutoCAD is the synthesis of two scientific papers, the idea being inspired by the manufacture processes.

In figure 7 it is presented comparatively an image obtained with a camera and a photographic representation of the planetary gear mechanism.



Figure 7: The image obtained with a camera (left) and the photographic representation in AutoCAD of the gear mechanism (right).

Mathematically speaking, this reflects real functioning cases of a vehicle with a hybrid propulsion system (heat engine, electric motor and electric generator).

The numerical results for the mechanism to function in transitory and permanent cases were obtained with a calculation program. This program is flexible, allowing not only to obtain the numerical results, but also to transfer the data to a program designed for graphical constructions.

For frequent functioning cases were compared the values experimentally obtained with those obtained using the mathematical model. The differences were lower the 5%.

The metallic frame with the mechanical system is presented in figure 8.



Figure 8: The mechanical system on the frame



Figure 9: Speed setting module

A second metallic frame (figure 9) was realized for mounting the batteries and the command module of the three-phased electric motor.

The power module SINAMICS allows the regulation of the asynchronous electric motor by modifying the voltage and varying the frequency. For a correct functioning the voltage data, maximum grip and power of the electric motor are inserted from the beginning in the CU240S command module. A particularity of the command module is that of retrieving the energy during the period when breaking the electric engine. The revolution can be both modified with a potentiometer or a computer by programming the functioning of the command module. Programming can be accomplished by setting switches, using the program and a computer directly plugged to the module or by an internet network.

EXPERIMENTAL DETERMINATIONS

The bench was coupled with two other existing benches. The coupling to the HOFFMAN bench with an electric break with tubular currents was realized by a universal joint and the coupling to the SCHENCK chassis dynamometer was realized by a homokinetic coupling with a tripod planetary.

The experimental determinations on the bench with an electric break with tubular currents had as main objective the analysis of the vibrations and sounds produced in operation.

From the frequency spectrograms we deduce the following:

For the housing of the mechanical system of coupling the power sources: the resonance box of the mechanical coupling system is at about 1000 Hz; in frequency spectrograms we found the frequencies caused by the gears engagement (revolution x number of teeth on the pinion x the number of satellites); the highest amplitude of a frequency is found at 2500 Hz.

For the frame of the bench: the heat engine induces harmonics on high frequencies; the structure of the frame has a side resonance of 2000Hz because of the constructive shape. This form is used only in this configuration, the frame being specially designed for the study of the two benches.

For the alternators: the vibrations are transmitted specially by mounting brackets; we have noticed some high frequencies because of the heat engine.

For the cylinder cap: the vibrations appear exclusively because of the excitation given by the heat engine; the values of the frequencies correspond to the resonance frequency of the cylinder cap.

For the fuel tank: in spectrograms we found a main resonance frequency of the fuel tank.

In terms of noise the following conclusions result:

In the case of bench functioning that it is driven by the heat and electric engine that are charged with nominal constant charge it is noticed: from the high frequencies spectrograms analysis results that there is noise due to engagement of the mechanical coupling system of the sources and ventilators of the electrical motors; predominates the low and medium frequencies; the global level isn't high since the system is not body-worked as it will be in the functionally version on a vehicle or stationary ensemble.

In the case of studying transitional arrangements we find that: from the analysis of the global noise level results that there are small level modifications during the measures that are held in a steady regime; the heat engine increases the global noise level with less over 10 dB.

The housing vibrations of the mechanical system have been theoretically studied by using the

equal sources method and by a dynamic analysis (in frequency) in Catia. The differences between the experimental results are low.

The experimental determinations on the chassis dynamometer had as main event measuring the cinematic and dynamic sizes of the mechanical system.

Being under construction (upgrading), in the hall in which the determinations were made the bench wasn't mounted below the ground level as in the project. There was made an ascension of the bench to make the coaxially between the shaft from the mechanical system and the fake deck with the rolling system.

The test report of the cinematic sizes has as main conclusion the functioning of the studied mechanism under the conditions of the firm's standards.

When the system is being used by the electric engine, the speed of the alternators is the speed of the electric motor multiplied with the gear ratio of 2.625. In this case the heat engine does not work and its speed is zero. When the system is being used by the heat engine, the speed of the electric motor and of the alternators is equal with that of the heat engine.

CONCLUSIONS

From those presented above it is noticed that planetary mechanisms with four elements can be used in joining thermo and electrical power sources. The advantages of these mechanisms are:

- a simple construction method,
- using this mechanism no longer needs the use of a gear box,
- there are not used breaks for blocking or unblocking some elements.

In terms of noise and vibrations, the mechanical system frames in the acceptable limits, the global noise being significantly lower then the one of a convention transmission.

REFERENCES

- [1] Pandrea, N., Popa D., Mecanisme. Teorie și aplicații CAD, Ed. Tehnică, București, 2000.
- [2] Popa, D., Chiroiu, V., L. Munteanu, J. Onisoru, A. Iarovici, On the modeling of hybrid systems, Proc. of the Romanian Academy, Series A: Mathematics, Physics, Technical Sciences, Information Science, vol. 8, nr. 1, 2007.
- [3] Teodorescu, P. P., Sisteme mecanice. Modele clasice, Ed. Tehnică, București, vol. 1-3, 1984-1988-1997.
- [4] Dudiță, FL, Mecanisme, Ed. Universitatea din Brașov, 1977.

SUMMARIES REZIMEA

¹ COMPARATIVE ANALYSIS ON MATHEMATICAL MODELS DESCRIBING VIBRATIONS OF AUTOMOTIVE INDEPENDENT SUSPENSIONS

Lilo Kunchev, Nikolay Pavlov, Technical University, Sofia

UDC: 519.87:629.012

Abstract

In the paper dynamic behaviour of two configurations independent suspensions for a car are investigated. For describing the mechanical system is used mathematical model based on vector-matrix algebra. The results from numerical experiments show laws of movement the suspended and nosuspended masses, theirs natural frequencies and theirs accelerations. The results for two kinds suspension are compared.

Key words: mathematical models, vibrations, natural frequencies, ride comfort.

UPOREDNA ANALIZA MATEMATIČKIH MODELA KOJI OPISUJU OSCILACIJE NEZAVISNIH SISTEMA ELASTIČNOG OSLANJANJA AUTOMOBILA

UDC: 519.87:629.012

Rezime: U radu je proučeno dinamičko ponašanje dve konfiguracije nezavisnih sistema elastičnog oslanjanja vozila. Za opisivanje mehaničkog sistema korišćen je matematički model zasnovan na vektorsko-matričnoj algebri. Rezultati numeričkih eksperimenata pokazuju zakone kretanja oslonjene i neoslonjene mase, njihove sopstvene frekvencije i njihova ubrzanja. Upoređeni su rezultati za dve vrste sistema elastičnog oslanjanja.

Ključne reči: matematički modeli, oscilacije, sopstvene frekvencije, udobnost vožnje.

¹ Received: May 2010.
Accepted: June 2010.

Primljen: U Maju, 2010.god.
Prihvaćen: U Junu, 2010.god.

COMPARATIVE ANALYSIS ON MATHEMATICAL MODELS DESCRIBING VIBRATIONS OF AUTOMOTIVE INDEPENDENT SUSPENSIONS

Lilo Kunchev¹, Nikolay Pavlov

UDC: 519.87:629.012

INTRODUCTION

Kinematical structure of the vehicle independent suspension with increased speeds of motion have been refined over time and today there are a large number of its variants - single, double, and more arm suspensions. Underlying all these are single arm suspensions [6].

The aim of this work is using the methods of vector mechanics to analyze the results for both types of suspensions for the generalization of the computing process, which form the basis of an automated computer program to select the elastic characteristics of the suspension. Numerical experiments are conducted with MATLAB.

THREE-DIMENSIONAL MATHEMATICAL MODELS OF ARM SUSPENSIONS DESCRIBING THE SMOOTHNESS OF MOTION WITH THE METHODS OF VECTOR MECHANICS

The most accurate description behavior of the vehicle is achieved by using three-dimensional mathematical models. The advantage of such schemes is that it is possible to investigate the relocation of the car and turns along the axes O_x , O_y and O_z of the coordinate system located in the center of gravity (i.e. all degrees of freedom) which is a premise for high accuracy in computation process [7]. Schemes of the models are shown in Figure 1 and Figure 2.

The systems under consideration consists suspended and nosuspended masses. The suspended masses include the masses of the elements of the car body, passengers and load. In the center of gravity is fixed local coordinate system $O_0x_0y_0z_0$. The suspension is implemented as a tire, arm, axle and other components are combined in one element which is hinged to the suspended masses [10].

Each of these elements is fixed to local coordinate system, respectively $O_1x_1y_1z_1$, $O_2x_2y_2z_2$, $O_3x_3y_3z_3$, $O_4x_4y_4z_4$. In the equilibrium position the axis of the all coordinate systems are parallel. All displacements of local coordinate systems are given to the absolute coordinate system $O_Ax_Ay_Az_A$. For systems of Fig. 1 and Fig. 2 make the following assumptions [11]:

- elements of the system are solids;

¹Corresponding author e-mail: lkunchev@tu-sofia.bg, Technical University, Sofia

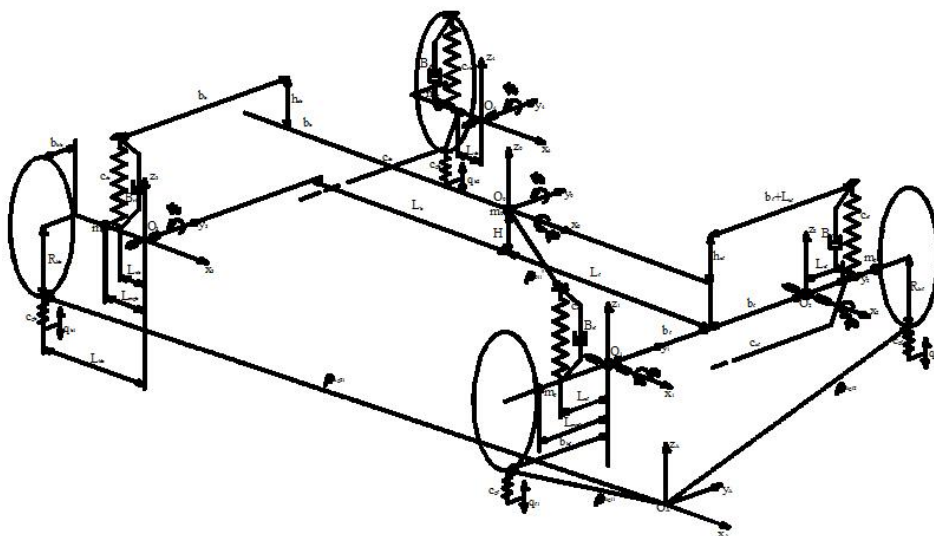


Figure 1: Kinematic scheme of a car with front transverse and rear longitudinal arms

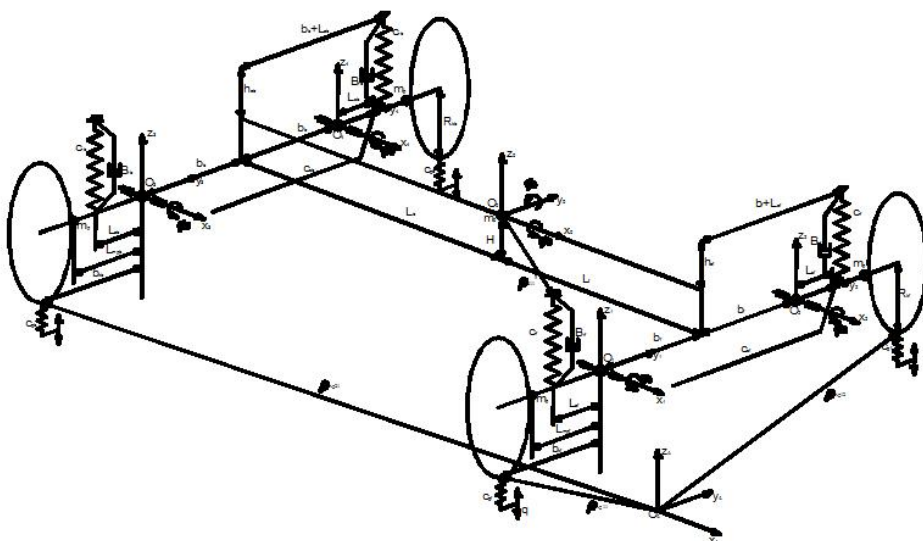


Figure 2: Kinematic scheme of a car with front and rear transverse arms

- anti-roll bars are massless and their stiffness is regarded as equivalent spring connected to the arms at point to a distance L_{sf} of the joint (hinge) of the front axle and L_{sb} of the joint of the rear axle;
- give an account damping and elastic properties of the main elements c_{rf} , c_{rb} , β_{rf} , β_{rb} , respectively, springs and shock absorbers the front and the rear axle, and the elasticity of the tire c_{gf} and c_{gb} the front and the rear axle;
- elastic and damping elements have linear characteristics;

- system is placed in a equilibrium position as the centers of gravity to the wheels lie on a horizontal axis. O_1y_1 axis coincides with the axis O_2y_2 , and O_3y_3 axis coincides with O_4y_4 .

For generalized coordinate systems are adopted:

- z_0 - linear displacement of the local coordinate system $O_0x_0y_0z_0$ to absolute $O_{Ax}A_yAZ_A$ on axis O_z ;
- φ_0, ψ_0 - angular displacement of the local coordinate system $O_0x_0y_0z_0$ to absolute $O_{Ax}A_yAZ_A$ respectively around the axes O_x and O_y ;
- φ_1 - angular displacement around the axis O_1x_1 of the coordinate system $O_1x_1y_1z_1$;
- φ_2 - angular displacement around the axis O_2x_2 of the coordinate system $O_2x_2y_2z_2$;
- φ_3 - angular displacement around the axis O_3x_3 of the coordinate system $O_3x_3y_3z_3$;
- φ_4 - angular displacement around the axis O_4x_4 of the coordinate system $O_4x_4y_4z_4$;
- ψ_3 - angular displacement around the axis O_3y_3 of the coordinate system $O_3x_3y_3z_3$;
- ψ_4 - angular displacement around the axis O_4y_4 of the coordinate system $O_4x_4y_4z_4$;

To find laws of motion in the absolute coordinate system $O_{Ax}A_yAZ_A$ is necessary to define the transition matrices of each local coordinate systems to the absolute.

Matrix of transition from $O_0x_0y_0z_0$ to $O_{Ax}A_yAZ_A$ for Fig. 1 and 2 is:

$$T_0^A = \begin{bmatrix} \cos \psi_0 & 0 & -\sin \psi_0 & 0 \\ -\sin \varphi_0 \cdot \sin \psi_0 & \cos \varphi_0 & -\sin \varphi_0 \cdot \cos \psi_0 & 0 \\ \cos \varphi_0 \cdot \sin \psi_0 & \sin \varphi_0 & \cos \varphi_0 \cdot \cos \psi_0 & z_0 \\ 0 & 0 & 0 & 1 \end{bmatrix} \quad (1)$$

x_0 and y_0 are zero because is consider only linear oscillation on axis Oz , i.e. only vertically; Matrix of transition from $O_1x_1y_1z_1, O_2x_2y_2z_2, O_3x_3y_3z_3, O_4x_4y_4z_4$, to $O_0x_0y_0z_0$ have a type:

For Figure 1:

$$T_1^0 = \begin{bmatrix} 1 & 0 & 0 & L_f \\ 0 & \cos \varphi_1 & -\sin \varphi_1 & -b_f \\ 0 & \sin \varphi_1 & \cos \varphi_1 & -H \\ 0 & 0 & 0 & 1 \end{bmatrix} \quad T_3^0 = \begin{bmatrix} \cos \psi_3 & 0 & -\sin \psi_3 & -L_b \\ 0 & 1 & 0 & -b_b \\ \sin \psi_3 & 0 & \cos \psi_3 & -H \\ 0 & 0 & 0 & 1 \end{bmatrix} \quad (2)$$

$$T_2^0 = \begin{bmatrix} 1 & 0 & 0 & L_f \\ 0 & \cos \varphi_2 & -\sin \varphi_2 & b_f \\ 0 & \sin \varphi_2 & \cos \varphi_2 & -H \\ 0 & 0 & 0 & 1 \end{bmatrix} \quad T_4^0 = \begin{bmatrix} \cos \psi_4 & 0 & -\sin \psi_4 & -L_b \\ 0 & 1 & 0 & b_b \\ \sin \psi_4 & 0 & \cos \psi_4 & -H \\ 0 & 0 & 0 & 1 \end{bmatrix}$$

For Figure 2 only T_3^0 and T_4^0 are different:

$$T_3^0 = \begin{bmatrix} 1 & 0 & 0 & -L_b \\ 0 & \cos \varphi_3 & -\sin \varphi_3 & -b_b \\ 0 & \sin \varphi_3 & \cos \varphi_3 & -H \\ 0 & 0 & 0 & 1 \end{bmatrix} \quad T_4^0 = \begin{bmatrix} 1 & 0 & 0 & -L_b \\ 0 & \cos \varphi_4 & -\sin \varphi_4 & b_b \\ 0 & \sin \varphi_4 & \cos \varphi_4 & -H \\ 0 & 0 & 0 & 1 \end{bmatrix} \quad (3)$$

After multiplying the matrices and simplify the resulting expressions for the components of the angular velocity of arms to three axes:

For Figure 1:

-front right arm:

$$\begin{aligned} \omega_{1x}^A &= \dot{\varphi}_0 + \dot{\varphi}_1 \cos \psi_0 & \omega_{1y}^A &= \dot{\psi}_0 \cos \varphi_0 + \dot{\varphi}_1 \sin \psi_0 \sin \varphi_0 \\ \omega_{1z}^A &= \dot{\varphi}_1 \sin \psi_0 \cos \varphi_0 - \dot{\psi}_0 \sin \varphi_0 \end{aligned} \quad (4)$$

After removal of terms of a higher order is received:

$$\omega_{1x}^A = \dot{\varphi}_0 + \dot{\varphi}_1 \quad \omega_{1y}^A = \dot{\psi}_0 \quad \omega_{1z}^A = 0 \quad (5)$$

Similarly to determine the angular velocities of the other arms:

-front left arm:

$$\omega_{2x}^A = \dot{\varphi}_0 + \dot{\varphi}_2 \quad \omega_{2y}^A = \dot{\psi}_0 \quad \omega_{2z}^A = 0 \quad (6)$$

- rear right arm:

$$\omega_{3x}^A = \dot{\varphi}_0 \quad \omega_{3y}^A = \dot{\psi}_0 + \dot{\psi}_3 \quad \omega_{3z}^A = 0 \quad (7)$$

- rear left arm:

$$\omega_{4x}^A = \dot{\varphi}_0 \quad \omega_{4y}^A = \dot{\psi}_0 + \dot{\psi}_4 \quad \omega_{4z}^A = 0 \quad (8)$$

For Figure 2 is only different angular speeds of the rear arms:

- rear right arm:

$$\omega_{3x}^A = \dot{\phi}_0 + \dot{\phi}_3 \quad \omega_{3y}^A = \dot{\psi}_0 \quad \omega_{3z}^A = 0 \quad (9)$$

- rear left arm:

$$\omega_{4x}^A = \dot{\phi}_0 + \dot{\phi}_4 \quad \omega_{4y}^A = \dot{\psi}_0 \quad \omega_{4z}^A = 0 \quad (10)$$

Kinetic energies of two systems are:

For Figure 1:

$$\begin{aligned} T = & \frac{1}{2} m_0 \dot{z}_0^2 + \frac{1}{2} J_{0x} \dot{\phi}_0^2 + \frac{1}{2} J_{0y} \dot{\psi}_0^2 + \frac{1}{2} J_{pxf} (\dot{\phi}_0 + \dot{\phi}_1)^2 + \frac{1}{2} J_{pxf} (\dot{\phi}_0 + \dot{\phi}_2)^2 + \\ & + \frac{1}{2} J_{pyb} (\dot{\psi}_0 + \dot{\psi}_3)^2 + \frac{1}{2} J_{pyb} (\dot{\psi}_0 + \dot{\psi}_4)^2 + \\ & + 2\left(\frac{1}{2} J_{pyf} \dot{\psi}_0^2\right) + 2\left(\frac{1}{2} J_{pxb} \dot{\phi}_0^2\right) + \frac{1}{2} m_p (\dot{z}_0 - (L_{mpf} + b_f) \dot{\phi}_0 + L_f \dot{\psi}_0 - L_{mpf} \dot{\phi}_1)^2 + \\ & + \frac{1}{2} m_p (\dot{z}_0 + (L_{mpf} + b_f) \dot{\phi}_0 + L_f \dot{\psi}_0 + L_{mpf} \dot{\phi}_2)^2 + \\ & + \frac{1}{2} m_p (\dot{z}_0 - b_b \dot{\phi}_0 - (L_{mpb} + L_b) \dot{\psi}_0 - L_{mpb} \dot{\psi}_3)^2 + \\ & + \frac{1}{2} m_p (\dot{z}_0 + b_b \dot{\phi}_0 - (L_{mpb} + L_b) \dot{\psi}_0 - L_{mpb} \dot{\psi}_4)^2 \end{aligned} \quad (11)$$

For Figure 2:

$$\begin{aligned} T = & \frac{1}{2} m_0 \dot{z}_0^2 + \frac{1}{2} J_{0x} \dot{\phi}_0^2 + \frac{1}{2} J_{0y} \dot{\psi}_0^2 + \frac{1}{2} J_{pxf} (\dot{\phi}_0 + \dot{\phi}_1)^2 + \\ & + \frac{1}{2} J_{pxf} (\dot{\phi}_0 + \dot{\phi}_2)^2 + \frac{1}{2} J_{pxb} (\dot{\phi}_0 + \dot{\phi}_3)^2 + \frac{1}{2} J_{pxb} (\dot{\phi}_0 + \dot{\phi}_4)^2 + \\ & + 2\left(\frac{1}{2} J_{pyf} \dot{\psi}_0^2\right) + 2\left(\frac{1}{2} J_{pyb} \dot{\psi}_0^2\right) + \frac{1}{2} m_p (\dot{z}_0 - (L_{mpf} + b_f) \dot{\phi}_0 + L_f \dot{\psi}_0 - L_{mpf} \dot{\phi}_1)^2 + \\ & + \frac{1}{2} m_p (\dot{z}_0 + (L_{mpf} + b_f) \dot{\phi}_0 + L_f \dot{\psi}_0 + L_{mpf} \dot{\phi}_2)^2 + \\ & + \frac{1}{2} m_p (\dot{z}_0 - (L_{mpb} + b_b) \dot{\phi}_0 - L_b \dot{\psi}_0 - L_{mpb} \dot{\psi}_3)^2 + \\ & + \frac{1}{2} m_p (\dot{z}_0 + (L_{mpb} + b_b) \dot{\phi}_0 - L_b \dot{\psi}_0 + L_{mpb} \dot{\psi}_4)^2 \end{aligned} \quad (12)$$

Potential energies of the two systems are:

For Figure 1:

$$\begin{aligned}
\Pi = & \frac{1}{2}c_{rf}(L_{cf}\varphi_1)^2 + \frac{1}{2}c_{rf}(-L_{cf}\varphi_2)^2 + \frac{1}{2}c_{rb}(L_{cb}\psi_3)^2 + \frac{1}{2}c_{rb}(L_{cb}\psi_4)^2 + \\
& + \frac{1}{2}c_{gz}(z_0 - (b_f + b_{kf})\varphi_0 + L_f\psi_0 - b_{kf}\varphi_1 - q_{f1})^2 + \\
& + \frac{1}{2}c_{gz}(z_0 + (b_f + b_{kf})\varphi_0 + L_f\psi_0 + b_{kf}\varphi_2 - q_{f2})^2 + \\
& + \frac{1}{2}c_{gz}(z_0 - (b_b + b_{kb})\varphi_0 - (L_b + L_{kb})\psi_0 - L_{kb}\psi_3 - q_{b1})^2 + \\
& + \frac{1}{2}c_{gz}(z_0 + (b_b + b_{kb})\varphi_0 - (L_b + L_{kb})\psi_0 - L_{kb}\psi_4 - q_{b2})^2 \\
& + \frac{1}{2}c_{sf}(-L_{sf}\varphi_1 - L_{sf}\varphi_2)^2 + \frac{1}{2}c_{sb}(-L_{sb}\psi_3 + L_{sb}\psi_4)^2
\end{aligned} \tag{13}$$

For Figure 2:

$$\begin{aligned}
\Pi = & \frac{1}{2}c_{rf}(L_{cf}\varphi_1)^2 + \frac{1}{2}c_{rf}(-L_{cf}\varphi_2)^2 + \frac{1}{2}c_{rb}(L_{cb}\varphi_3)^2 + \\
& + \frac{1}{2}c_{rb}(-L_{cb}\varphi_4)^2 + \frac{1}{2}c_{gz}(z_0 - (b_f + b_{kf})\varphi_0 + L_f\psi_0 - b_{kf}\varphi_1 - q_{f1})^2 + \\
& + \frac{1}{2}c_{gz}(z_0 + (b_f + b_{kf})\varphi_0 + L_f\psi_0 + b_{kf}\varphi_2 - q_{f2})^2 + \\
& + \frac{1}{2}c_{gz}(z_0 - (b_b + b_{kb})\varphi_0 - L_b\psi_0 - b_{kb}\varphi_3 - q_{b1})^2 + \\
& + \frac{1}{2}c_{gz}(z_0 + (b_b + b_{kb})\varphi_0 - L_b\psi_0 + b_{kb}\varphi_4 - q_{b2})^2 \\
& + \frac{1}{2}c_{sf}(-L_{sf}\varphi_1 - L_{sf}\varphi_2)^2 + \frac{1}{2}c_{sb}(-L_{sb}\varphi_3 - L_{sb}\varphi_4)^2
\end{aligned} \tag{14}$$

The Rayleigh's functions are:

For Figure 1:

$$R = \frac{1}{2}\beta_{rf}(L_{cf}\dot{\varphi}_1)^2 + \frac{1}{2}\beta_{rf}(-L_{cf}\dot{\varphi}_2)^2 + \frac{1}{2}\beta_{rb}(L_{cb}\dot{\psi}_3)^2 + \frac{1}{2}\beta_{rb}(L_{cb}\dot{\psi}_4)^2 \tag{15}$$

For Figure 2:

$$R = \frac{1}{2}\beta_{rf}(L_{cf}\dot{\varphi}_1)^2 + \frac{1}{2}\beta_{rf}(-L_{cf}\dot{\varphi}_2)^2 + \frac{1}{2}\beta_{rb}(L_{cb}\dot{\varphi}_3)^2 + \frac{1}{2}\beta_{rb}(-L_{cb}\dot{\varphi}_4)^2 \tag{16}$$

After applying Lagrange's equation of 2nd kind:

$$\frac{d}{dt}\left(\frac{\partial \Gamma}{\partial \dot{q}}\right) - \left(\frac{\partial \Gamma}{\partial q}\right) = -\left(\frac{\partial \Pi}{\partial q}\right) - \left(\frac{\partial R}{\partial \dot{q}}\right) \tag{17}$$

For equations describing the laws of motion of the system is valid:

$$[M]\ddot{q} + [B]\dot{q} + [C]q = [F] \tag{18}$$

- [M] is the matrix of inertia that is symmetrical with the main diagonal with dimension 7x7 and she has the following form:

$m_p + 4m_b$	0	$2m_p L_r$ $2m_p(L_{mpb} + L_b)$ $2m_p L_r - 2m_p b_b$	$-m_p L_{maf}$	$m_p L_{maf}$	$-m_p L_{mab}$	$-m_p L_{mab}$ $m_p L_{mab}$
$-m_p L_{mab}$	$J_{ox} + 2J_{oxf} + 2J_{oxb} + 2m_p b_b^2 + 2m_p(L_{maf} + b_f)^2$ $J_{ox} + 2J_{oxf} + 2J_{oxb} + 2m_p(L_{maf} + b_f)^2 + 2m_p(L_{mpb} + b_b)^2$	0	$J_{oxf} + m_p L_{maf}(L_{maf} + b_f)$	$J_{oxf} + m_p L_{maf}(L_{maf} + b_f)$	$m_p b_b L_{mab}$	$-m_p b_b L_{mab}$
$2m_p L_r - 2m_p(L_{mpb} + L_b)$	0	$J_{ov} + 2J_{ovb} + 2J_{ovf} + 2m_p L_r^2 + 2m_p(L_{mpb} + L_b)^2$ $J_{ov} + 2J_{ovb} + 2J_{ovf} + 2m_p L_r^2 + 2m_p(L_{mpb} + L_b)^2$	$-m_p L_{maf}$	$m_p L_{maf}$	$J_{ovb} + m_p L_{mpb}(L_{mpb} + L_b)$	$J_{ovb} + m_p L_{mpb}(L_{mpb} + L_b)$
$2m_p L_r - 2m_p L_b$	0	$J_{ov} + 2J_{ovb} + 2J_{ovf} + 2m_p L_r^2 + 2m_p(L_{mpb} + L_b)^2$ $J_{ov} + 2J_{ovb} + 2J_{ovf} + 2m_p L_r^2 + 2m_p(L_{mpb} + L_b)^2$	$-m_p L_{maf}$	$m_p L_{maf}$	$m_p L_b L_{mab}$	$-m_p L_b L_{mab}$
$-m_p L_{maf}$	$J_{oxf} + m_p L_{maf}(L_{maf} + b_f)$	$-m_p L_{maf}$	$J_{oxf} + m_p L_{maf}^2$	0	0	0
$m_p L_{maf}$	$J_{oxf} + m_p L_{maf}(L_{maf} + b_f)$	$m_p L_{maf}$	0	$J_{oxf} + m_p L_{maf}^2$	0	0
$-m_p L_{mab}$	$m_p b_b L_{mab}$	$J_{ovb} + m_p L_{mpb}(L_{mpb} + L_b)$	0	0	$J_{ovb} + m_p L_{mpb}^2$	0
$-m_p L_{mab}$	$-m_p b_b L_{mab}$	$J_{ovb} + m_p L_{mpb}(L_{mpb} + L_b)$	0	0	$J_{ovb} + m_p L_{mpb}^2$	0
$m_p L_{mab}$	$J_{ovb} + m_p L_{mpb}(L_{mpb} + L_b)$	$-m_p L_b L_{mab}$	0	0	0	$J_{ovb} + m_p L_{mpb}^2$

- [C] is the matrix of elasticity, which is also symmetric and has dimension 7x7

$4C_{gz}$	0	$2C_{gz}L_f - 2C_{gz}(L_g + L_{kb})$	$-C_{gz}b_{kf}$	$C_{gz}b_{kf}$	$-C_{gz}L_{kb}$	$-C_{gz}L_{kb}$
0	$2C_{gz}(b_f + b_{kf}) + 2C_{gz}(b_b + b_{kb})^2$	0	$C_{gz}b_{kf}(b_f + b_{kf})$	$C_{gz}b_{kf}(b_f + b_{kf})$	$C_{gz}L_{kb}(b_b + b_{kb})$	$C_{gz}b_{kb}(b_b + b_{kb})$
$2C_{gz}L_f - 2C_{gz}(L_g + L_{kb})$	0	$2C_{gz}L_f^2 + 2C_{gz}(L_b + L_{kb})^2$	$-C_{gz}b_{kf}L_f$	$C_{gz}b_{kf}L_f$	$C_{gz}L_{kb}$	$C_{gz}L_{kb}(L_b + L_{kb})$
$-C_{gz}b_{kf}$	$C_{gz}b_{kf}(b_f + b_{kf})$	$-C_{gz}b_{kf}L_f$	$C_{kf}L_{kf}^2 + C_{gz}b_{kf}^2 + C_{sf}L_{sf}^2$	$C_{sf}L_{sf}^2$	0	0
$C_{gz}b_{kf}$	$C_{gz}b_{kf}(b_f + b_{kf})$	$C_{gz}b_{kf}L_f$	$C_{sf}L_{sf}^2$	$C_{kf}L_{kf}^2 + C_{gz}b_{kf}^2 + C_{sf}L_{sf}^2$	0	0
$-C_{gz}L_{kb}$	$C_{gz}L_{kb}(b_b + b_{kb})$	$C_{gz}L_{kb}(L_b + L_{kb})$	0	0	$C_{fb}L_{fb}^2 + C_{gz}$	$-C_{sb}L_{sb}^2$
$C_{gz}b_{kb}$	$C_{gz}b_{kb}(b_b + b_{kb})$	$C_{gz}b_{kb}L_b$	0	0	$C_{fb}L_{fb} + C_{gz}b_{kb}^2 + C_{sb}L_{sb}^2$	$C_{sb}L_{sb}^2$
$-C_{gz}L_{kb}$	$-C_{gz}L_{kb}(b_b + b_{kb})$	$C_{gz}L_{kb}(L_b + L_{kb})$	0	0	$-C_{sb}L_{sb}^2$	$C_{fb}L_{fb}^2 + C_{gz}$
$C_{gz}b_{kb}$	$C_{gz}b_{kb}(b_b + b_{kb})$	$-C_{gz}b_{kb}L_b$	0	0	$C_{sb}L_{sb}^2$	$C_{fb}L_{fb} + C_{gz}b_{kb}^2 + C_{sb}L_{sb}^2$

Cells colored in Lt Dwn Diagonal refer to the system of Figure 1 and those in gray (light) of Figure 2.

- [B] is the matrix of dissipative forces, showing the influence of damper - symmetric with dimension 7x7:

0	0	0	0	0	0	0
0	0	0	0	0	0	0
0	0	0	0	0	0	0
0	0	0	$\beta_{rf} \cdot L_{cf}^2$	0	0	0
0	0	0	0	$\beta_{rf} \cdot L_{cf}^2$	0	0
0	0	0	0	0	$\beta_{rb} \cdot L_{cb}^2$	0
0	0	0	0	0	0	$\beta_{rb} \cdot L_{cb}^2$

To obtain natural frequencies of its system equations are presented in Cauchy normal form:

$$y + Ly = 0 \tag{19}$$

Where L is:

$$L = \begin{bmatrix} M^{-1}B & M^{-1}C \\ I & O \end{bmatrix} \tag{20}$$

The output parameters of the system are vibration displacement, vibration velocity, vibration acceleration and they are obtained from the equations:

$$y + Ly = Y \tag{21}$$

Where Y is:

$$Y = \begin{bmatrix} M^{-1}F(t) \\ O \end{bmatrix} \tag{22}$$

After integration of the system using the method of Runge - Kutta receive all decisions in a given time interval.

NUMERICAL INVESTIGATIONS

The main parameters and their numerical values are shown in table 1:

Table 1:

№	Parameter	Symbol	Value
1.	Suspended masses	m_0	1400 kg
2.	Nosuspended masses	m_p	30 kg
3.	Moment of inertia of the sprung masses around longitudinal axis (x-axis)	J_{0x}	550 kg.m ²
4.	Moment of inertia of the sprung masses around transverse axis (y-axis)	J_{0y}	2000 kg.m ²
5.	Moment of inertia of the unsprung masses on the front axle around x-axis	J_{pxf}	5 kg.m ²
6.	Moment of inertia of the unsprung masses on the rear axle around x-axis	J_{pxb}	2 kg.m ²
7.	Moment of inertia of the unsprung masses on the front axle around y-axis	J_{pyf}	2 kg.m ²
8.	Moment of inertia of the unsprung masses on the rear axle around y-axis	J_{pyb}	5 kg.m ²
9.	Vertical co-ordinate of the center of gravity of the unsprung masses in relation to joint of the arms	H	0,4 m
10.	Horizontal co-ordinate of the center of gravity of the unsprung masses in relation to joint of the front arms	b_f	0,4 m
11.	Horizontal co-ordinate of the center of gravity of the unsprung masses in relation to joint of the rear arms	b_b	0,6 m
12.	Distance from the center of gravity to the front axle	L_f	1,1 m
13.	Distance from the center of gravity to the rear axle	L_b	1,5 m
14.	Length of the front arm	b_{kf}	0,42 m
15.	Length of the rear arm	L_{kb}	0,42 m
16.	Distance from the contact point of the rear wheel to joint of the arm	b_{kb}	0,2 m
17.	Distance from the center of gravity of the front(f) and the rear(b) arm to the respective joint	L_{mp}	0,4 m
18.	Distance from fixing point of the front(f) and the rear(b) main elastic element to the respective joint	L_c	0,3 m
19.	Distance from fixing point of the front(f) and the rear(b) anti-roll bar to the respective joint	L_s	0,28 m
20.	Radius of the front(f) and the rear(b) wheels	R_k	0,26 m
21.	Stiffness coefficient of the main elastic elements of the front axle	c_{rf}	25000 N/m

№	Parameter	Symbol	Value
22.	Stiffness coefficient of the main elastic elements of the rear axle	c_{rb}	25000 N/m
23.	Stiffness coefficient of the tyre	c_{gz}	125000 N/m
24.	Stiffness coefficient of the anti-roll bars of the front(f) and the rear(b) axle	c_s	20000 N/m
25.	Damping coefficient of the front(f) and the rear(b) shock absorbers	β_r	1900 N.s/m

The parameters are not measured by authors and are taken from literary sources cited below.

Natural frequencies of the systems:

0.8099 Hz (for Fig.1) / 0.9839 Hz (for Fig. 2) - frequency of linear oscillations of suspended masses on z-axis;

1.6722 Hz / 1.7286 Hz - frequency of angular oscillation of the sprung masses around x-axis;

1.1740 Hz / 0.8367 Hz - frequency of angular oscillation of the sprung masses around y-axis;

7.8614 and 7.8506 Hz / 7.8593 and 7.8832 Hz - angular frequency of the front arms;

8.3490 and 8.3100 Hz / 8.2327 and 8.3100 Hz - angular frequency of the rear arms;

Disturbing actions in the system are sinusoidal and are attached in the center of the contact patch of the tire with the road. They have the following form:

$$q = q_0 (1 - \cos(vt)) \quad (23)$$

$q_0 = 0,02$ m - height of the amplitude of roughness;

v - circular frequency of the disturbing action:

$$v = \frac{2\pi.V}{S}, \text{ rad/s} \quad (24)$$

The frequency of the disturbing action expressed in hertz:

$$v = \frac{1}{2\pi} \frac{2\pi.V}{S}, \text{ Hz} \quad (25)$$

V - velocity of the car, m / s;

S - wavelength, m.

As the maximum accelerations are important, the investigated of the behavior of individual

elements of the system was conducted at a frequency effects similar to their natural frequencies. The results obtained for some of the accelerations are shown in figures below:

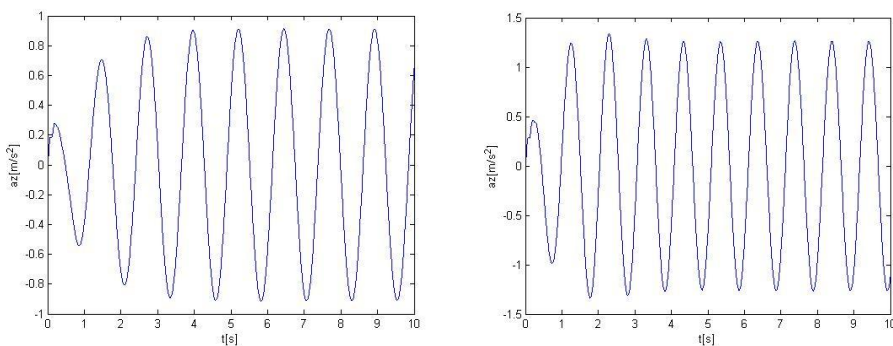


Figure 3: Linear acceleration of sprung masses on z-axis respectively of the models in Figure 1 and 2

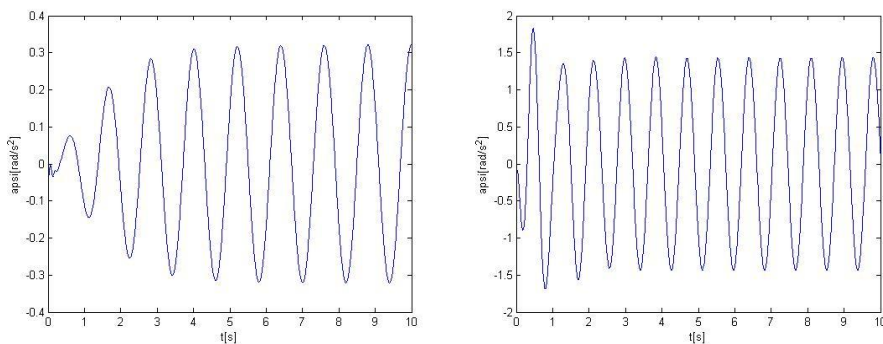


Figure 4: Angular acceleration of suspended masses on y-axis respectively of the models in Figure 1 and 2

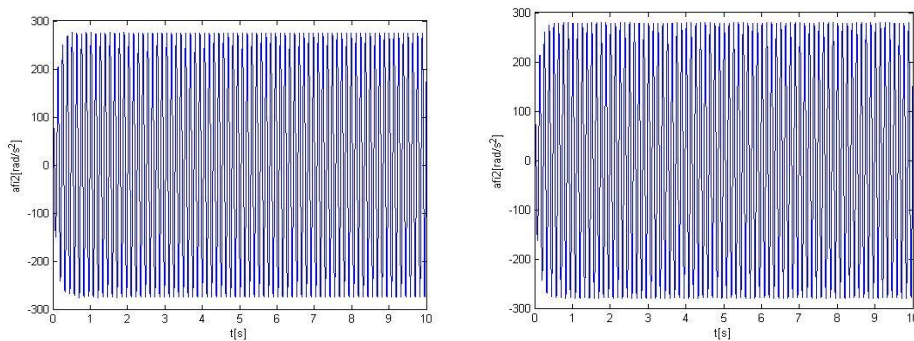


Figure 5: Angular acceleration of the front left arm of Figure 1 and 2

CONCLUSION

The generalization of the matrix of both automotive suspension may be used to create automated software to set its computing part and thus to accelerate the work in choosing the type of suspension and its elastic parameters.

ACKNOWLEDGEMENT

This work is a part of the research project to support of PhD students № 102ПД021-4 funded by Research Centre at Technical University – Sofia.

REFERENCES

- [1] Demic, M., Diligenski, D., Demic, I., Demic, M. A method of vehicle active suspension design. Springer – Verlag, 2006.
- [2] Ellis, J.R. Vehicle Dynamics. London Business Books Limited, 1975.
- [3] Genta, G. Motor Vehicle Dynamics. Word Scientific, 1997.
- [4] Hirshberg, W. Fahrzeugdynamic. 1997.
- [5] Katzov, D., D. Hlebarski. Kinematiks of the turn of wheel vehicle with account of the tires and influence of the suspension. International Journal of Pure and Applied Mathematics, Vol 25, № 2, 2005.
- [6] Kunchev, L.P., G.M. Yanachkov. Изследване динамичното поведение на раменно окачване.
- [7] Kunchev, L.P., G.M. Yanachkov. Моделиране плавността на движение на автомобил с еднораменно окачване. trans&MOTAUTO'05, Велико Търново, 2005.
- [8] Русев, Р., П. Партинов, Т. Тодоров. Свободни трептения на системата трансмисия – окачване. Петнадесети национален семинар „Динамика на механични системи”, Варна, 1990.
- [9] Яначков, Г.М. Изследване динамичното поведение на предно раменно окачване тип Макферсон, trans&MOTAUTO'06.
- [10] Kunchev, L.P., G.M. Yanachkov. Изследване динамичното поведение на автомобил с раменно окачване. trans&MOTAUTO'06.
- [11] Kunchev, L., G. Yanachkov. Comparison analyze on the theoretical mechanic mathematical models, describing arm suspensions. MVM, Kragujevac, 4th – 6th October 2006, Serbia.

SUMMARIES REZIMEA

¹ NUMERICAL SIMULATION OF AIR FLOW THROUGH TWO DIFFERENT SHAPED AIR VENTS

Catalin-Adrian Neacsu, Automobile Dacia - Group Renault Romania

Mariana Ivanescu, Ion Tabacu, University of Pitesti, Automotive Department, 1,

Tg. din Vale, Pitesti, Romania

UDC: 519.872:697.94]:629.113

Abstract

Air conditioning vents shape represents one of the cockpit features that give style and also functionality in modern cars. In this paper our aim is to analyze the functional shape of the vents regarding their influence to the air flow through them using CFD software. For the simulation, we will use two different shaped air vents, both with the same functional area.

They will have the fins opened at maximum position, thus permitting the biggest air flow.

Using Ansys Fluent CFD software we will simulate the air flow distribution through this two different shape vents, and we will compare the results for both cases in terms of air speed distribution at different distances from the outlets extremities.

Key words: numerical simulation, air flow, CFD software, vents, Fluent.

NUMERIČKA SIMULACIJA PROTOKA VAZDUHA KROZ DVA VENTILACIONA OTVORA RAZLIČITOG OBLIKA

UDC: 519.872:697.94]:629.113

Rezime: Oblik ventilacionih otvora klima-uređaja predstavlja jednu od karakteristika kabine koja odslikava stil i funkcionalnost kod savremenih vozila. U ovom radu, naš cilj je analiza funkcionalnog oblika otvora u pogledu njegovog uticaja na protok vazduha, korišćenjem CFD softvera. U simulacijama ćemo koristiti dva ventilaciona otvora različitog oblika, pri čemu oba otvora imaju istu funkcionalnu površinu. Oni će imati maksimalno otvorena krilca, čime se dozvoljava najveći protok vazduha.

Korišćenjem Ansys Fluent CFD softver, simuliraćemo raspodelu protoka vazduha kroz ova dva otvora različitog oblika i upoređićemo rezultate u oba slučaja preko raspodele brzine vazduha na različitoj udaljenosti od izlaza.

Ključne reči: numerička simulacija, protok vazduha, CFD softver, otvori, Fluent.

¹ Received: May 2010.

Accepted: June 2010.

Primljen: U Maju, 2010.god.

Prihvaćen: U Junu, 2010.god.

NUMERICAL SIMULATION OF AIR FLOW THROUGH TWO DIFFERENT SHAPED AIR VENTS

Catalin-Adrian Neacsu¹, Mariana Ivanescu, Ion Tabacu

UDC: 519.872:697.94]:629.113

INTRODUCTION

Most car manufacturers give a lot of attention in the shape of interior components such as dashboard, steering wheel, different setting knobs, seats and even air inlets. The latter represent a challenge because they must allow the car occupants to easily direct the air flow and also to provide a good distribution of air inside the cabin [1], [4].

In the recent years, one tool that is often used in the field of airflow numerical simulation is represented by the computational fluid dynamics (CFD). It has proved its efficiency in various applications including also the automotive field. We can find CFD used in applications concerning the airflow around cars, inside car airflow, and also the simulation of the engine functioning.

In our paper, we will use CFD to simulate the air flow through two different shaped air flow vents with the same external area and to analyze the air distribution at various distances, starting from 100 to 500mm from the outlet of the air vent. For the numerical simulation we will use the Fluent 6.3.26 software, because it's proved capability to solve problems concerning the air flow. The 3D model of the air vents was created in Catia V5, using measurements taken from the physical parts, and the finite element model used was created using the Beta Cae ANSA software.

BRIEF INTRODUCTION TO FLUENT

Fluent code contains all the physical capabilities needed to model flow, turbulence, heat transfer and reactions for industrial applications[2],[6]. It uses a finite volume approach to solve the equations governing the flow and is widely used in numerical simulations of different flow conditions of various complexities. It is chosen in this study because its proven capability and validity in flows similar to those investigated here. The turbulent flow fields are calculated by solving the Reynolds averaged three-dimensional Navier-Stokes equations along with the continuity equation (1) and (2)[3],[5],[7],[8],[9].

¹ Corresponding author e-mail: catalin.neacsu@renault.com; Automobile Dacia - Group Renault Romania

This paper was written in the project „**Doctoral and post-doctoral programmes in support of research**”, co-financed by EUROPEAN SOCIAL FUND through The Sectoral Operational Programme for Human Resources Development

(1):

$$\begin{aligned} \frac{\partial \bar{u}}{\partial t} + \bar{u} \frac{\partial \bar{u}}{\partial x} + \bar{v} \frac{\partial \bar{u}}{\partial y} + \bar{w} \frac{\partial \bar{u}}{\partial z} &= X - \frac{1}{\rho} \frac{\partial \bar{p}}{\partial x} + \nu \Delta \bar{u} + \frac{1}{\rho} \left(\frac{\partial}{\partial x} (-\rho \overline{u'u'}) + \frac{\partial}{\partial y} (-\rho \overline{v'u'}) + \frac{\partial}{\partial z} (-\rho \overline{w'u'}) \right) \\ \frac{\partial \bar{v}}{\partial t} + \bar{u} \frac{\partial \bar{v}}{\partial x} + \bar{v} \frac{\partial \bar{v}}{\partial y} + \bar{w} \frac{\partial \bar{v}}{\partial z} &= Y - \frac{1}{\rho} \frac{\partial \bar{p}}{\partial y} + \nu \Delta \bar{v} + \frac{1}{\rho} \left(\frac{\partial}{\partial x} (-\rho \overline{u'v'}) + \frac{\partial}{\partial y} (-\rho \overline{v'v'}) + \frac{\partial}{\partial z} (-\rho \overline{w'v'}) \right) \\ \frac{\partial \bar{w}}{\partial t} + \bar{u} \frac{\partial \bar{w}}{\partial x} + \bar{v} \frac{\partial \bar{w}}{\partial y} + \bar{w} \frac{\partial \bar{w}}{\partial z} &= Z - \frac{1}{\rho} \frac{\partial \bar{p}}{\partial z} + \nu \Delta \bar{w} + \frac{1}{\rho} \left(\frac{\partial}{\partial x} (-\rho \overline{u'w'}) + \frac{\partial}{\partial y} (-\rho \overline{v'w'}) + \frac{\partial}{\partial z} (-\rho \overline{w'w'}) \right) \end{aligned}$$

$$\frac{\partial \bar{u}}{\partial x} + \frac{\partial \bar{v}}{\partial y} + \frac{\partial \bar{w}}{\partial z} = 0 \quad (2)$$

To solve the equations (1) and (2) have been developed various approaches, one of the most used being the use of two equations model. The k-ε model is one of the most used turbulence model, and it includes two extra transport equations to represent the turbulent properties of the flow. This allows a two equation model to account for history effects like convection and diffusion of turbulent energy.

The first transported variable is turbulent kinetic energy, k and the second transported variable in this case is the turbulent dissipation, ε. It is the variable that determines the scale of the turbulence, whereas the first variable, k, determines the energy in the turbulence[6].

In the Fluent software the user can choose from three types of k- ε model solver: Standard, RNG and Realizable, each one with its own mathematical expression, and in our simulation we will use the Realizable k- ε model, because it satisfies specific constraints that make the model more consistent with the physics of turbulent flows, and give more accurate results than the Standard k- ε model[6].

GEOMETRY PREPARATION

Starting from the measurements taken from the real pieces we have realized the 3D model of the air inlets using CATIA software, and we have scaled them to have the same frontal area, which will be of 0.006m², the surface being the same for the air flow entrance in the inlet.

After the CAD creation, we have used the Beta CAE Ansa to obtain the surface mesh of the air inlets, mesh that can be seen in figure 1 and 2.

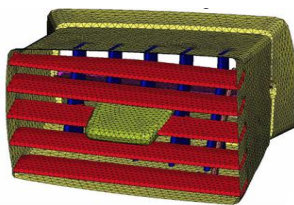


Figure 1: Rectangular shaped air inlet

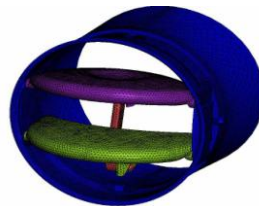


Figure 2: Round shaped air inlet

In table 1 we can see a short description of the finite element model for both types of vents.

Table 1: Description of the finite element model

Shape	Rectangular	Round
Type of elements	Only tria	Only tria
Number of elements	~ 60000	~ 40000
Medium size of mesh	1mm	1.2mm

Comparing those two air vents, we can observe that the rectangular shaped vent is more complex, having a lot more components than the rounded shaped vent, thus giving us a bigger number of triangular elements on the domain, with about 50% more than the round shaped model.

Because we will want to analyse the flow at different distances from the air vent, we must construct an additional geometry, in which the air will flow, and this will be our post-processing domain. The shape of the geometry is given in figure 3 (with the rectangular vent integrated), and it will be an extruded isoscel trapeze with the base of 800mm, the short edge of 200mm and a height of 1000mm. The extrusion will be of 800mm, the centre of inlet being positioned at the centre of the upper face, as we can see in figure 3. The same shape is used also in [1].

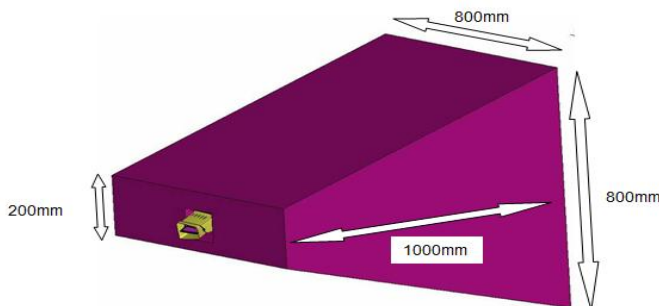


Figure 3: Computational domain

With the computational domain defined and the vent included, we will create the volume discretization of domain obtaining around 0.75×10^6 elements for the rounded shape vent and around 1.2×10^6 elements for the rectangular shaped vent.

BOUNDARY CONDITIONS AND FLUENT SET-UP

Because we will simulate numerically the air flow through the vents we will need to define the boundary conditions at the inlets, thus being given by a flow rate. To determine the type of flow, we must also compute the Reynolds number for each type of flow, with the formula (3) [5].

$$Re = \frac{QD_H}{\nu A} \tag{3}$$

where: Q – Volumetric flow rate (m³/s)
 D_H – Hydraulic diameter (m)
 ν – Kinematic viscosity (m²/s) - 15.68x10⁻⁶ m²/s for air
 A – Cross sectional area of the entry domain (m²)

The values for the flow rate and Reynolds number for each flow can be seen in table 2.

Table 2: Flow rate with corresponding Reynolds number

Air flow rate(m ³ /s)	0.075		0.040	
Type of inlet	Rectangular	Round	Rectangular	Round
Area (m ²)	0.0057	0.0060	0.0057	0.0060
Hydraulic diameter(m)	0.307	0.273	0.307	0.273
Reynolds(Re) number	257619	217633	137397	116071
Type of flow (based on Re)	Turbulent	Turbulent	Turbulent	Turbulent

Based on the Reynolds number, we can establish that the flow is turbulent; we can now set up the Fluent solver. We will use, as we mentioned, the Realizable k- ε model for solving the turbulent flow, and we will define the inlet boundary condition as a mass-flow inlet and the outlet as a pressure outlet. For the mass flow inlet we will use the values in the table 2, as for the outlet we will consider the atmospheric pressure.

RESULTS

With the specified boundary conditions, we will have four simulations, two for each type of vent. We will analyse the air flow magnitude on central axis of the boundary domain (intersection of the planes Y=0 and Z=0) and also the distribution on sectional planes as we can see in figure 4.

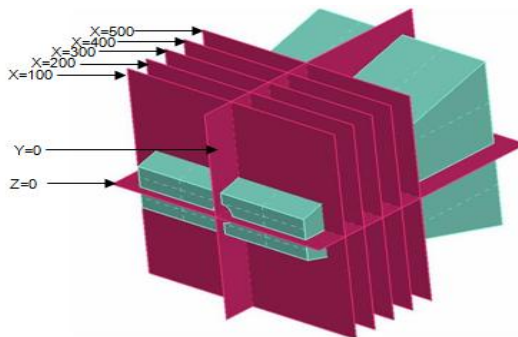
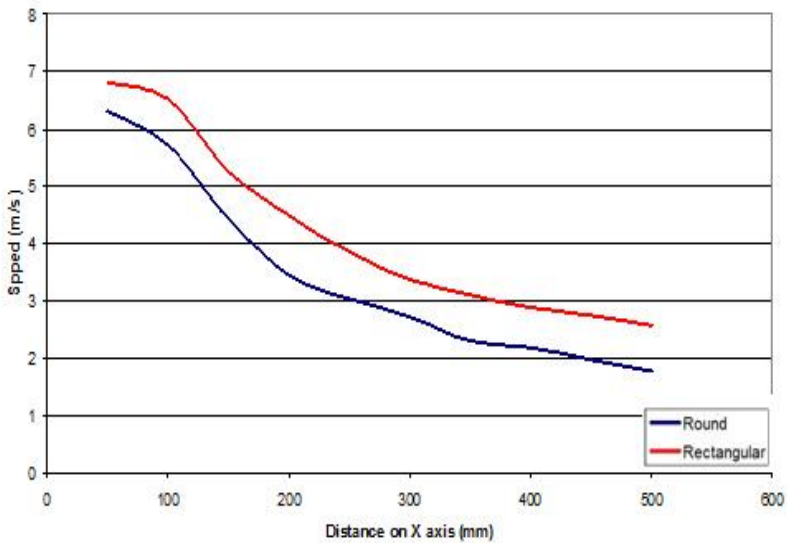


Figure 4: Post-processing planes

In table 3 we can see the velocity values obtained for the speed in all four simulations and in figure 5 we can see the graphs of velocity.

Table 3: Velocities along the domain centreline

Air flow rate(m ³ /s)	0.075			0.040		
Type of inlet	Rectangular	Round	Difference	Rectangular	Round	Difference
	Speed(m/s)		(m/s)	Speed(m/s)		(m/s)
x= 50mm	6.81	6.30	+0.51	12.79	11.72	+1.07
x=100mm	6.51	5.73	+0.78	12.41	10.75	+1.66
x=150mm	5.25	4.41	+0.84	9.85	8.24	+1.61
x=200mm	4.49	3.43	+1.06	8.43	6.40	+2.03
x=250mm	3.86	3.02	+0.84	7.24	5.60	+1.64
x=300mm	3.36	2.72	+0.64	6.31	5.06	+1.25
x=350mm	3.09	2.31	+0.78	5.82	4.31	+1.51
x=400mm	2.88	2.19	+0.69	5.43	4.07	+1.36
x=450mm	2.73	1.95	+0.78	5.13	3.60	+1.53
x=500mm	2.57	1.78	+0.79	4.84	3.28	+1.56



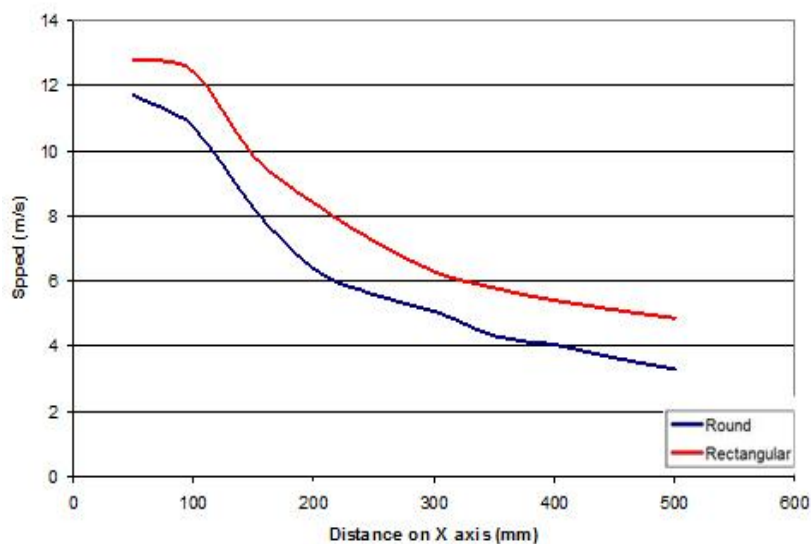


Figure 5: Graphics of velocity on the centreline ($0.04\text{m}^3/\text{s}$ left; $0.075\text{m}^3/\text{s}$ right)

Analyzing the obtained results, we observe a difference between the results obtained with the rectangular shaped vent and round shaped vent. This difference can be explained by the different obstructed area from the internal components of the air vents. The internal components of the round shaped air inlet obstruct an area of 0.0016m^2 whilst the internal components of the rectangular shaped 0.0021m^2 , this can be seen in figure 6. The area obstructed refers to the projected area of the last fins on the perpendicular plane.

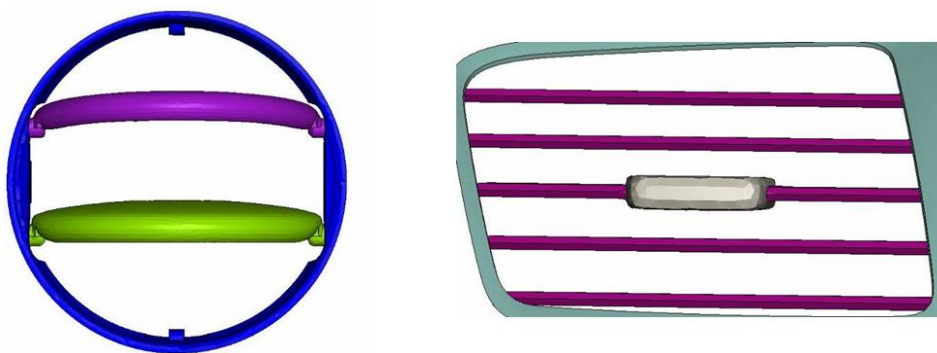


Figure 6: Obstructed area for both type of vents

In figures 7 and 8 we can see the cartographies of air distribution in the sectional planes $y=0\text{mm}$ and $z=0\text{mm}$ for the two flow rates given, and in figure 9 and 10 we can see the air distribution in planes x from 100 to 500 mm.

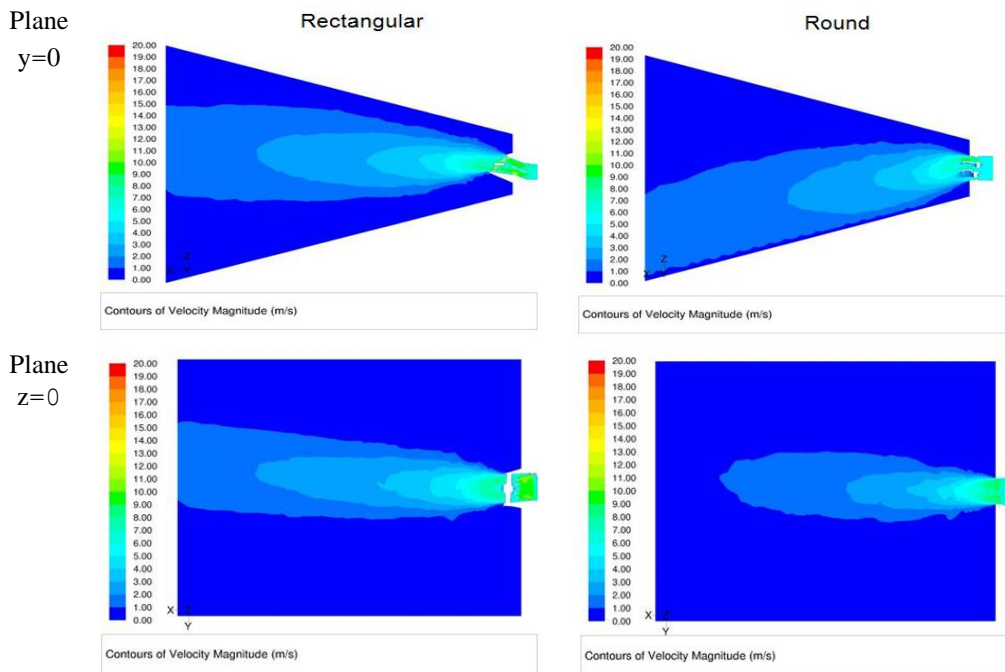


Figure 7: Cartographies of velocities in planes y and z for an air flow rate of $0.040\text{m}^3/\text{s}$

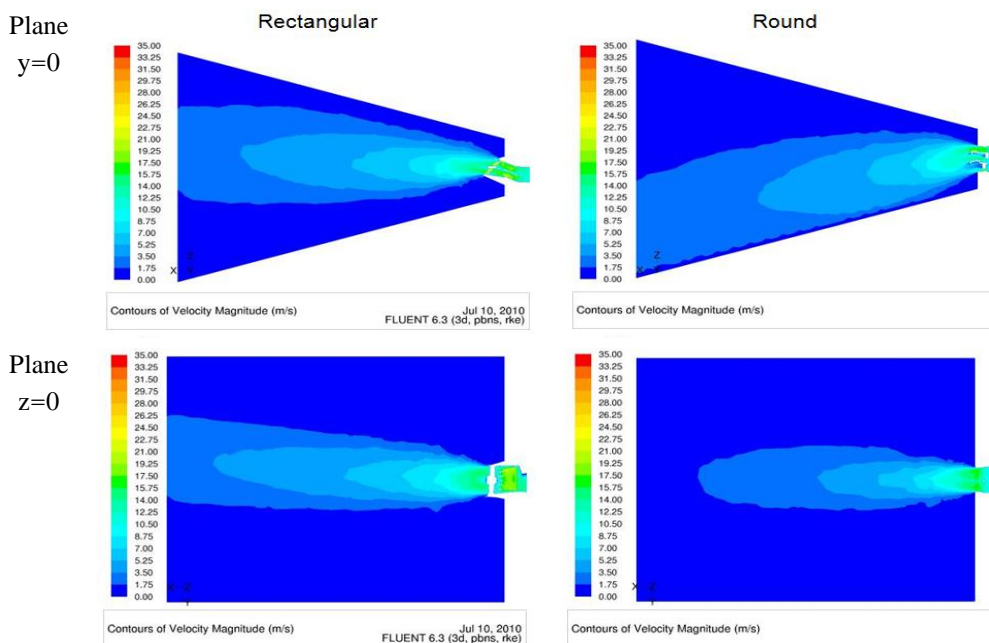


Figure 8: Cartographies of velocities in planes y and z for an air flow rate of $0.075\text{m}^3/\text{s}$

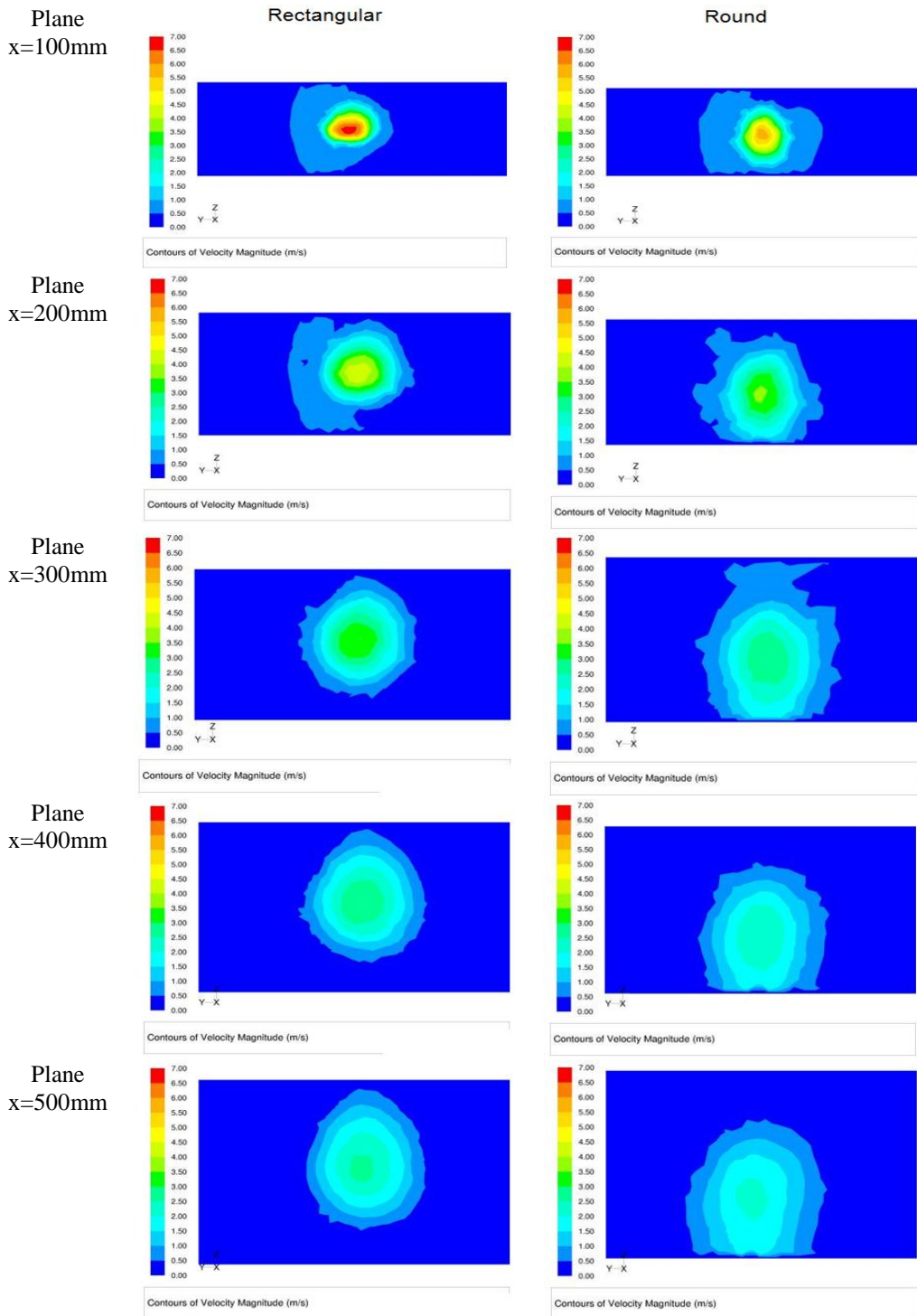


Figure 9: Cartographies of velocities in planes x from 100 to 500mm for an air flow rate of $0.040m^3/s$

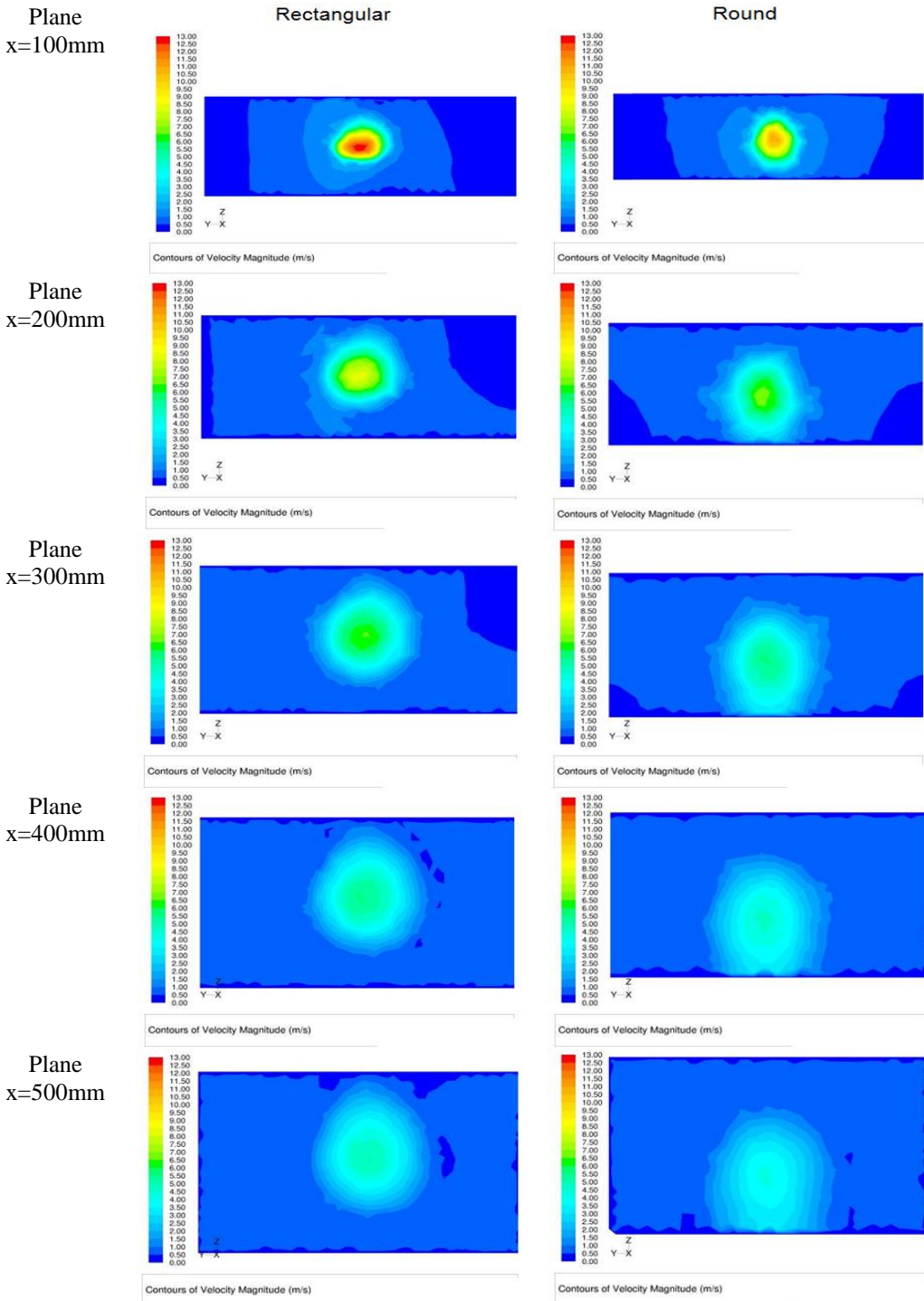


Figure 10: Cartographies of velocities in planes x from 100 to 500mm for an air flow rate of $0.075\text{m}^3/\text{s}$

Also, from figures 7 to 10 we can see that in the case of the rounded shaped vent, the air is directed mainly downward, although the upper side of the fins is parallel with the plane $Z=0$. The path can be explained by the existence of a rounded surface at the outer extremities, as we can see in figure 11. Here we can see the vectors in the plane $Y=0$, and we can observe that the vectors are directed slightly downward.

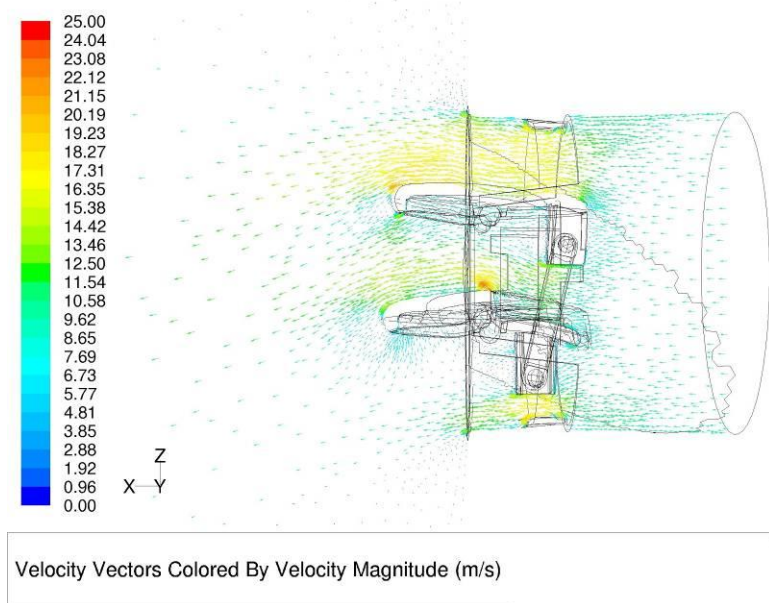


Figure 11: Velocity vectors at the exit of the inlet in the plane with XOY

CONCLUSIONS

Analyzing the obtained results, we can see that beside the aesthetic role, the air vents also have an role in the air distribution inside car cockpit, different shape giving us different results.

The first conclusion is that for the same frontal area, the exit speed of air is greater in the case of the rectangular inlet than the round, for the same quantity of air entered. To obtain the same velocity of air for the rectangular and round air inlets we have multiple opportunities:

- increasing the area of the rectangular inlet, thus giving us also a bigger area covered by the air inside the cockpit;
- decreasing the quantity of air needed in the case of the rectangular vent, this giving us a gain in the energy needed for the ventilation system.

Also, analyzing the results obtained in the case of the round air inlet vent, we can observe that small details of the fins can change the trajectory of the exiting air.

REFERENCES

- [1] Axelsson Niklas and Enwald Hans, “Accuracy in flow simulation of climate control – Part I: The air distribution system”, SAE 1999-01-1200
- [2] Broboana D., Muntean T., Balan C.: “ Mecanica fluidelor cu FLUENT-vol 1”, Ed. Politehnica, Bucuresti, 2005
- [3] Cebeci T., Shao J.P., Kafyeke F., Laurendeau E., “Computational Fluid Dynamics for Engineers”, Horizons Publishing Inc. USA, 2005
- [4] Currle J., Maue J. “Numerical study of the influence of air vent area and air mass flux on the thermal comfort of car occupants”, SAE 2000-01-0980
- [5] Florea J., Panaitescu V. : “ Mecanica Fluidelor” – Editura Didactica si Pedagogica Bucuresti, 1979
- [6] Fluent 6.3.26 Users Guide
- [7] Hirsch C. “Numerical computation of internal and external flows”, Volume 1, Fundamentals of Computational Fluid Dynamics, Butterworth-Heinemann, 2007
- [8] Petrila T.,Trif D.: “ Basics of fluid mechanics and introduction to computational fluid dynamics “, Springer, 2004
- [9] White F.M. “Fluid Mechanics”, 4th ed. The McGraw Companies, 2001

MVM Editorial Board
University of Kragujevac
Faculty of Mechanical Engineering
Sestre Janjić 6, 34000 Kragujevac, Serbia
Tel.: +381/34/335990; Tel.: 336002; Fax: + 381/34/333192
www.mvm.mfkg.kg.ac.rs